

Geochemistry, Geophysics, Geosystems



RESEARCH ARTICLE

10.1029/2025GC012488

Key Points:

- Dynamic subduction models capture feedback between thermal state, mantle wedge serpentinization, interface weakening, and plate speeds
- Sediment lubricates the plate interface indirectly by providing water that reacts with the mantle wedge to produce weak serpentinite
- Serpentinization promotes faster plate speeds, especially after early subduction and sufficient serpentinite accumulation

Supporting Information:

Supporting Information may be found in the online version of this article.

Correspondence to:

A. F. Holt and R. K. Stoner, aholt@miami.edu; ryankstoner@gmail.com

Citation:

Stoner, R. K., Holt, A. F., Epstein, G. S., Guevara, V. E., & Condit, C. B. (2025). Emergent feedbacks between progressive serpentinization, interface weakening, and subduction rates. *Geochemistry*, *Geophysics, Geosystems*, 26, e2025GC012488. https://doi.org/10.1029/2025GC012488

Received 3 JUN 2025 Accepted 19 OCT 2025

Author Contributions:

Conceptualization: R. K. Stoner,
A. F. Holt, V. E. Guevara, C. B. Condit
Data curation: R. K. Stoner
Formal analysis: R. K. Stoner, A. F. Holt,
G. S. Epstein, V. E. Guevara, C. B. Condit
Funding acquisition: A. F. Holt,
V. E. Guevara, C. B. Condit
Investigation: R. K. Stoner, A. F. Holt,
G. S. Epstein, V. E. Guevara, C. B. Condit
Methodology: R. K. Stoner, A. F. Holt,
G. S. Epstein, V. E. Guevara

© 2025 The Author(s). Geochemistry, Geophysics, Geosystems published by Wiley Periodicals LLC on behalf of American Geophysical Union.
This is an open access article under the terms of the Creative Commons Attribution License, which permits use, distribution and reproduction in any medium, provided the original work is properly cited.

Emergent Feedbacks Between Progressive Serpentinization, Interface Weakening, and Subduction Rates

R. K. Stoner¹, A. F. Holt¹, G. S. Epstein^{1,2}, V. E. Guevara³, and C. B. Condit²

¹Rosenstiel School of Marine, Atmospheric, and Earth Science, University of Miami, Miami, FL, USA, ²Department of Earth and Space Sciences, University of Washington, Seattle, WA, USA, ³Geology Department, Amherst College, Amherst. MA, USA

Abstract During subduction, the downgoing oceanic crust is exposed to high temperatures in the mantle wedge, causing volatile-bearing minerals to break down and release hydrous fluids into the forearc. These fluids percolate upwards, reacting with the mantle wedge to form hydrated ultramafic lithologies, including serpentinite. To accurately track the fate and impact of water on the forearc, we develop time-dependent models that self-consistently capture both serpentinite ingrowth and the associated rheological weakening of the plate interface. Unlike many subduction models that investigate forearc serpentinization and prescribe plate velocities, geometries, or steady-state conditions, our approach allows plates to evolve dynamically without predefined velocities or geometries. During subduction infancy, serpentinite accumulates rapidly. As subduction matures, serpentinite ingrowth decreases, and more serpentinite is also dragged downward by the slab. To elucidate the links between subduction dynamics and serpentinization, we consider variations in serpentinite strength and hydration state of the incoming plate. Subducting fully water-saturated sediments yield ~3× greater forearc serpentinite than within the moderately hydrated reference case. The water-saturated case produces a weaker interface and, in turn, subduction zone convergence rates ~40% higher than in an endmember case with anhydrous sediment. A lower serpentinite strength also produces higher convergence rates despite more downdragging of serpentinite from the forearc. We find that hydrous sediments not only lubricate the interface directly by weakening it, as previously suggested, but also by dehydrating and releasing water that produces weak serpentinite in the mantle wedge, with such feedback only able to be captured within fully coupled dynamic models.

Plain Language Summary We develop and analyze computer models of subduction where plate forces and speeds can change freely and where water movement is tracked. Water moving upwards from the plate interface during subduction forms weak rocks called serpentinites. We find these weak serpentinites can lubricate the interface between plates and speed up subduction over time. This is also important because previous research proposed that sediments may change subduction speeds. Instead, sediments release water that is needed for weak serpentinites to form that could also lubricate the interfaces of subducting plates.

1. Introduction

The mechanical and compositional properties of the plate interface underpin a range of subduction behaviors, including deformation (Behr & Bürgmann, 2021; Shreve & Cloos, 1986), rock exhumation (Agard et al., 2018; Gerya et al., 2002), deep mantle hydration (Faccenda et al., 2012; Magni et al., 2014; Rüpke et al., 2004), and volatile budgets in the mantle wedge (Hacker, 2008; Ito et al., 1983; Iwamori, 2007; Schmidt & Poli, 1998; van Keken et al., 2011). Volatiles are liberated from the downgoing plate, migrate upwards, and, depending on the fluid composition and pressure-temperature (P-T) conditions, may be bound in weak hydrous lithologies, such as serpentinite (Abers et al., 2017; Epstein et al., 2024; Hyndman & Peacock, 2003; Peacock, 1990). Moreover, subduction zones are dynamic systems, and therefore both P-T conditions and associated fluid release and storage change over time. To investigate these interrelated processes, we develop numerical subduction models to estimate the impacts of dehydration and/or hydration patterns on large-scale subduction zone evolution.

Previous studies have made strides in predicting slab water release and mantle wedge hydration by coupling the thermal fields from time-invariant, kinematically driven subduction models—characterized by fixed slab dips and convergence rates—with metamorphic phase equilibria calculations (Abers et al., 2017; Hacker, 2008; Hyndman & Peacock, 2003; van Keken et al., 2011). However, both geological (Agard et al., 2012; Cloos, 1985;

STONER ET AL. 1 of 23

15252027, 2025, 11, Downloaded from https://agupubs.onlinelibrary.wiley.com/doi/10.1029/2025GC012488, Wiley Online Library on [16/11/2025]. See the Terms and Conditions

Project administration: A. F. Holt,
V. E. Guevara, C. B. Condit
Resources: R. K. Stoner, A. F. Holt,
V. E. Guevara
Software: R. K. Stoner, A. F. Holt,
G. S. Epstein
Supervision: A. F. Holt
Validation: R. K. Stoner, G. S. Epstein
Visualization: R. K. Stoner, A. F. Holt,
G. S. Epstein
Writing – original draft: R. K. Stoner
Writing – review & editing: R. K. Stoner,
A. F. Holt, G. S. Epstein, V. E. Guevara,
C. B. Condit

Dragovic et al., 2020; Platt, 1975) and numerical studies (Molnar & England, 1990; Peacock, 1990; Wang et al., 1995) predict that slab temperatures, and hence dehydration patterns evolve over time. These thermal changes create transients in mantle wedge hydration and dehydration, which time-invariant models cannot capture. For example, rapid changes in slabtop temperatures can arise due to time-dependent kinematic properties that make up the "thermal parameter" (e.g., Kirby et al., 1996; van Keken et al., 2011), such as convergence rates, which can evolve even over million-year timescales (Faccenna et al., 2001; Sdrolias & Müller, 2006). These changes are self-consistently captured in "dynamic" subduction models, where plate forces and velocities are allowed to evolve freely without external forcing. These models self-consistently produce a highly timedependent slab thermal structure (e.g., Billen & Arredondo, 2018; Kincaid & Sacks, 1997) and hence timedependent water release (Holt & Condit, 2021; Zhou & Wada, 2021). Fluctuations in water release also affect water storage: a postprocessing of Holt and Condit's (2021) dynamic subduction thermal models revealed that slab water release and water storage in mantle wedge serpentinites almost always exceed those predicted by fixedgeometry, constant-velocity subduction models (Abers et al., 2017) because dynamic models capture the hotter, earlier stages of subduction (Epstein et al., 2024). However, in a dynamic context, the release and storage of water is also likely to impact the slab evolution itself, because weak hydrous minerals accumulating near the plate interface influence the mechanical and rheological properties of the interface.

While previous studies have incorporated time-dependent hydration of the mantle wedge and associated serpentinite ingrowth, they have typically prescribed plate speeds and/or subduction zone geometries. These assumptions, in turn, neglect the dynamic evolution of subduction zone properties, such as convergence rate and dip, and hence the resulting impact of changes in these kinematic properties on slab and wedge temperatures, dehydration/hydration, and vice versa. Such studies have successfully captured the impacts of serpentinization in contexts such as high/ultra-high pressure rock exhumation (Gerya et al., 2002; Gerya & Stöckhert, 2006), arc magmatism (Gerya & Meilick, 2011; Gorczyk et al., 2007; Nikolaeva et al., 2008), mantle wedge dynamics (Kerswell et al., 2021; Li et al., 2019; Wada et al., 2008), and steady-state water budgets (Abers et al., 2017; Wada et al., 2012). Other studies have illuminated some of the feedback between serpentinization and large-scale subduction using models by implementing wedge hydration and milder kinematic prescriptions, such as prescribed boundary conditions for part of the model duration (Balázs et al., 2022; Li et al., 2019), or prescribed velocities on only one of the two plates (Arcay et al., 2005, 2006). Some notable exceptions include the studies of Nakao et al. (2016, 2018), which employed dynamic models to explore the significant impact of wedge hydration on subduction properties, such as convergence rates and slab dips, but focused on hydrous weakening in a generalized sense (i.e., not serpentinite-specific). Ritter et al. (2024) also implemented wedge hydration and serpentinization in the context of dynamically evolving subduction but with a specific focus on subduction initiation. However, taken together, most previous subduction modeling studies have thus integrated only specific feedback related to slab dehydration and mantle wedge serpentinization within kinematically driven models, or within dynamic models, explored generic fluid-related mantle weakening and/or focused on specific phases of subduction. Therefore, here we conduct a comprehensive examination of the interplay between forearc hydration and serpentinization, interface properties, and their combined influence on dynamically evolving subduction properties.

One example of how serpentinization may impact large-scale subduction is by modifying the strength of the plate interface, which, in turn, affects the subduction zone force balance and hence plate velocities. Such feedback between slab behavior, such as plate speeds, and variable interface strength has been explored within fully dynamic models for interfaces with uniform lithologies at the slabtop (Behr et al., 2022; Čížková & Bina, 2013). For example, weak subducting materials, including sediment (Behr & Becker, 2018; Lamb, 2006; Shreve & Cloos, 1986) and altered oceanic crust (Kimura & Ludden, 1995), can impact subduction zone plate speeds by reducing the net subducting-resisting shear stress exerted on the slab by the interface (Conrad & Hager, 1999). However, in contrast to a potentially steady input of sediment or oceanic crust, weak hydrous minerals, such as serpentine (Moore & Lockner, 2004; Wada & Wang, 2009) or talc (Boneh et al., 2023; Horn & Deere, 1962), accumulate in the mantle wedge over time as hydrous fluids are released from the downgoing slab. These minerals have been shown to weaken the plate interface in models with hydration of the mantle wedge (Arcay et al., 2005; Gerya et al., 2008; Nakao et al., 2016, 2018). Therefore, we expect serpentinite accumulation in the mantle wedge to cause a time-dependent feedback loop with subduction kinematics, such as plate speeds, because serpentinite stability in the mantle wedge is highly dependent on the time-evolving P-T conditions. These conditions are modulated by advection driven by plate speeds, which are, in turn, influenced by the strength of weak materials at

STONER ET AL. 2 of 23

5252027, 2025, 11, Downloaded from https://agupubs.onlinelibrary.wiley.com/doi/10.1029/2025GC012488, Wiley Online Library on [16/11/2025]. See the Term

the plate interface, including serpentinite. Thus, examining feedback between slab thermal structure, serpentinization, and plate dynamics requires the coupling of temperature-dependent dehydration and hydration with freely evolving model subduction zones.

To reveal the scope of emergent feedbacks between serpentinization and large-scale subduction zone evolution, we present dynamic models of subduction with weak serpentinite ingrowth near the plate interface. We isolate the impacts of slab dehydration, wedge hydration via serpentinization, and associated strength changes of the plate interface by examining numerical models with varying interface yielding properties and hydration states of the downgoing slab crust. By simulating serpentinite formation and its feedback on temperature, water release, and plate interface lubrication, these models directly capture and quantify time-dependent subduction zone strength and dynamics.

2. Materials and Methods

We develop 2-D ocean-ocean subduction models using the ASPECT finite element code (ASPECT v2.5.0-pre; Bangerth et al., 2023; Gassmöller et al., 2018; Heister et al., 2017; Kronbichler et al., 2012; Rose et al., 2017). We solve for the conservation of momentum, mass, and energy, respectively. The incompressible Boussinesq approximation is used for mass conservation, and we do not incorporate radioactive or shear heating:

$$-\nabla \cdot 2\eta \dot{\boldsymbol{\varepsilon}}(\boldsymbol{v}) + \nabla p = \rho \boldsymbol{g} \tag{1}$$

$$\nabla \cdot \mathbf{v} = 0 \tag{2}$$

$$\rho C_p \left(\frac{\partial T}{\partial t} + \mathbf{v} \cdot \nabla T \right) - k \nabla^2 T = 0 \tag{3}$$

Where η is viscosity, $\dot{\boldsymbol{e}}$ is strain rate, \boldsymbol{v} is velocity, p is the total pressure, ρ is density, and \boldsymbol{g} is gravitational acceleration. In the heat conservation equation C_p is the specific heat capacity, T is temperature, and k is thermal conductivity. Individual lithologies are represented by compositional fields that are advected by the flow field. Advection of these compositional fields is treated by an additional advection equation (Equation 4) for each field c to the preceding equations (Equations 1–3):

$$\frac{\partial c_i}{\partial t} + \mathbf{v} \cdot \nabla c_i = q_i \tag{4}$$

A source reaction term q is used to update compositional quantities (c_i) , such as the ingrowth of serpentinite.

We consider an initially 100-million-year-old oceanic plate subducting below a younger, 10-million-year-old overriding plate to ensure self-sustained subduction (Figure 1). Spreading centers are located 500 km from either boundary of the domain at the margins of both the subducting and overriding plates. An initial curved section of the subducting plate is included that extends to a depth of 50 km and 145 km inboard of the trench. The model domain dimensions are $5,800 \times 1,450$ km. All other associated parameters are listed in Table 1 and Table S1.

The models are dynamic, and plate forces and geometries are allowed to evolve freely. In terms of thermal structure and (non-interface) mechanical properties, the models are similar to those of Holt and Condit (2021). However, unlike in this previous work, the present models contain a free surface with surface diffusion at the upper boundary. This free surface is allowed to isostatically equilibrate for 100 timesteps prior to the main 50 million year-long model run (Figure 1). A diffusion coefficient of 10^{-7} m²/s is used to prevent extreme topographic gradients and hence increase numerical stability (e.g., Rose et al., 2017; Grima and Becker, 2024). Except for this free surface upper boundary, free-slip boundaries are enforced elsewhere. A constant mantle potential temperature of 1,421°C is used (GDH1 plate cooling model: Stein & Stein, 1992). Constant temperatures are enforced at the bottom (1,421°C) and top (0°C) of the domain. Insulated (no heat flux) boundary conditions are enforced on the left and right sides of the domain.

ASPECT's adaptive mesh refinement functionality is used to locally increase model resolution in regions with high strain rates and high temperatures or within regions containing threshold quantities of the lithologies (or

STONER ET AL. 3 of 23

15252027, 2025, 11, Downloaded from https://agupubs.onlinelibrary.wiley.com/doi/10.1029/2025GC012488, Wiley Online Library on [16/11/2025]. See the Terms and Conditions (https://onlinelibrary.wiley.com/terms/

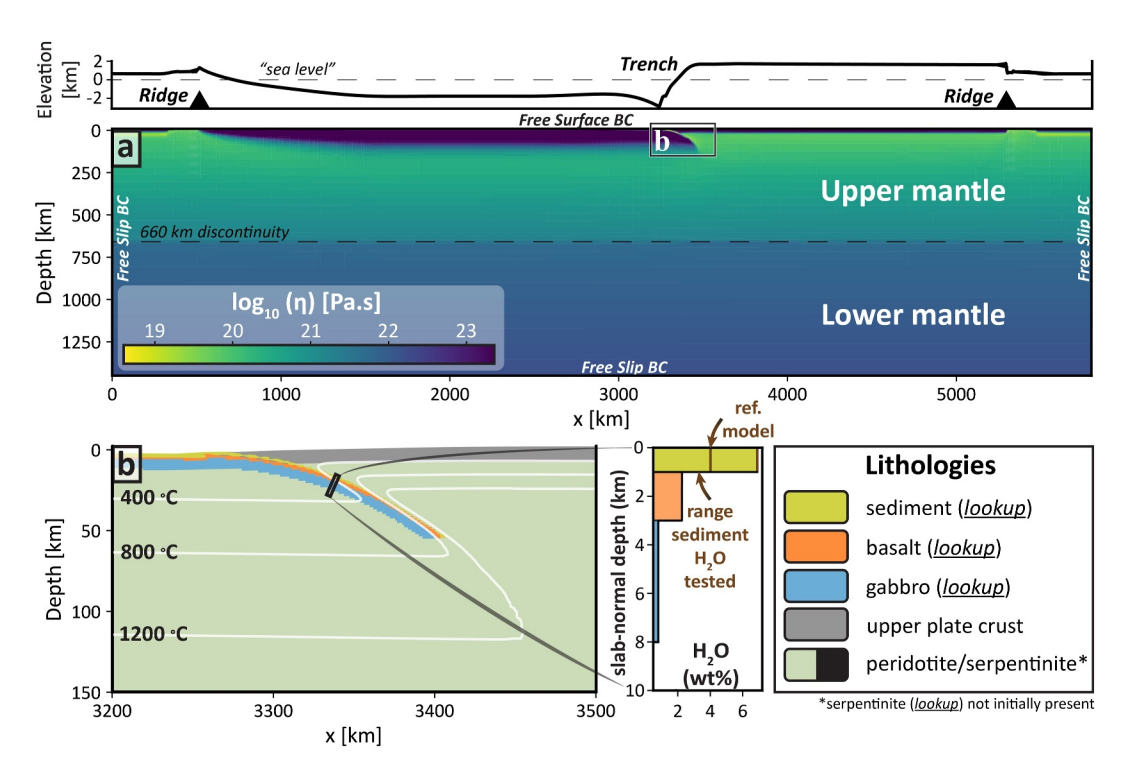


Figure 1. Model setup showing the initial viscosity field and initial, isostatically equilibrated, topography (a) with a zoom-in of the subduction interface region (b). The lithologies/compositions of the downgoing crust are also shown, with thicknesses and the range of explored sediment H₂O concentrations (see Methods Sections 2.1 and 2.2). As illustrated, some compositions use lookup tables to assign rheology and density (see Table 1).

compositions, i.e. Equation 4) that make up the plate interface region. Refinement levels are chosen so that there is a minimum resolution of \sim 230 km and a maximum resolution of \sim 1.3 km (e.g., within the plate interface). We also set the resolution near the 660 km discontinuity to have a grid size of \sim 2.6 km. In the reference model, the initial number of degrees of freedom is \sim 2,900,000, and the final number of degrees of freedom at the end of the run, after increasing amounts of mesh refinement, is \sim 9,400,000.

2.1. Phase Stability

Our model crust is constructed as a simplified version of the oceanic crust described in Jarrard (2003) and is overlain by pelagic sediment with a composition from Hacker (2008). The crust is composed of, in order of increasing depth away from the slabtop, 1 km of pelagic sediment, 2 km of metabasalt, and 5 km of metagabbro (Figure 1b). Assuming a 100 Myr old oceanic crust, the metabasalt initial H₂O content is calculated as an average of the H₂O content of 300 m of upper volcanic extrusives (6.04 wt. %), 300 m of lower extrusives (4.1 wt. %), and 1,600 m of sheeted dykes (1.76 wt. %) for an H₂O content of 2.3 wt. % distributed homogeneously throughout the 2 km of slab upper crust. The metagabbro has 0.79 wt. % H₂O, while the pelagic sediment has 6.89 wt. % H₂O because we infer it is fully saturated. However, to explore the impact of variable H₂O inputs, we examine a range of sediment H₂O concentrations relative to this reference value (Figure 1b). No initial pore fluid is included for any of the crust; all H₂O is initially mineralogically bound (Table 1). Hydration of abyssal serpentinite is not considered because abyssal serpentinite dehydration occurs beyond serpentinite stability in the wedge, as expected given that slab interiors are cooler than slab tops (Epstein et al., 2024), though km-scale layers of abyssal serpentinites with very low density may resist subduction (Nakao et al., 2018).

Phase equilibria modeling is used to track the stable mineral assemblage in the various slab lithologies as a function of P-T conditions. Density and bound water content for all crustal compositions are determined directly from the phase equilibria results (Figures S1 and S2 in Supporting Information S1), and viscosities are calculated within ASPECT using flow laws associated with the dominant calculated mineral modes (see Section 2.3). Fluid released during metamorphic dehydration reactions (assumed to be pure H₂O) is determined by monitoring

STONER ET AL. 4 of 23

15252027, 2025, 11, Downloaded from https://agupubs.onlinelibrary.wiley.com/doi/10.1029/2025GC012488, Wiley Online Library on [16/11/2025]. See the Terms and Conditions (https://onlinelibrary.wiley.com/

 Table 1

 Model Parameters Associated With Individual Compositions

Composition	Flow law ^a	$A \\ [Pa^{-n}.s^{-1}]$	<i>n</i>	E_a [kJ/mol]	<i>r</i>	V [cm ³ mol ⁻¹]	$ au_0 ext{ (LTP)}^{ extbf{b}} ext{ [GPa]}$	p (LTP) ^b	(LTP) ^b	Melt	C ₀ [MPa]	μ _{eff}	Initial H ₂ O [wt. %]	Reference density [kg/m³]
sediment	wet quartz ^c	6.31×10^{-36}	4	135	1	0	_	_		_	1	0.02	6.89	Lookup
metabasalt	wet quartz ^c	6.31×10^{-36}	4	135	1	0	_	_	_	_	1	0.04	2.32	Lookup
	amphibolite ^d	6.94×10^{-27}	3.7	244	0	0	_	_	_	27				
	eclogite ^e	1.99×10^{-18}	3.5	403	0	27.2	_	_	_	27				
metagabbro	wet quartz ^c	6.31×10^{-36}	4	135	0	0	_	_	_	_	20	0.04	0.79	Lookup
	$amphibolite^{\displaystyle \frac{d}{t}}$	6.94×10^{-27}	3.7	244	1	0	_	_	_	27				
	eclogite ^e	1.99×10^{-18}	3.5	403	0	27.2	_	_	_	27				
serpentinite	serpentinite ^{b,f}	4.37×10^{-22}	2	86.3	_	_	2.42	1	1.18	_	1	0.01- 0.06	_	Lookup
mantle	dry olivine (disl. creep) ^g	9.15×10^{-20}	3.5	540	0	12	_	_	_	_	20	0.36	0	3,300
	dry olivine (diff. creep) ^g	9.6×10^{-12}	1	300	0	4	_	_	_	_				
overriding plate oceanic crust	same as mantle	_	_	_	_	_	_	_	_	_		0.36	0	2,800
yielding region	same as mantle	_	_	_	-	_	_	_	_	_		0	0	3,300
lower mantle	20× olivine diff. creep	4.8×10^{-13}	1	300	0		_	_	_	_		0.36	0	3,300

^aEquation 5. ^bBurdette & Hirth (2022) and Fildes and Billen (2025). ^cHirth et al. (2001). ^dHacker & Christie (1990). ^cZhang & Green (2007). ^fEquation 11. ^gKarato & Wu (1993).

changes in the bound water content of the mineral assemblage during prograde metamorphism, similar to previous studies (Abers et al., 2017; Condit et al., 2020; Epstein et al., 2024; van Keken et al., 2011; Wada et al., 2012). Once free water is produced, it is tracked as described in the following section. We use "water" throughout the text interchangeably with $\rm H_2O$ even though such fluid may be supercritical in part of the domain. Phase equilibria modeling and the production of data tables used by ASPECT were performed using Perple_X version 7.0.1 (Connolly, 2005). All thermodynamic calculations were carried out in the system $\rm Na_2O$ -CaO- $\rm K_2O$ -FeO-MgO-Al $\rm _2O_3$ -SiO $\rm _2$ -H $\rm _2O$. We use the thermodynamic database of Holland and Powell (2011) and Pitzer and Sterner (1994) for the fluid equation of state. Solid solution models for all calculations are provided in the Supporting Information (Table S2).

2.2. H₂O Transport

Although the mantle wedge is not initially hydrated, the hydrated crust from the downgoing plate encounters relatively hotter conditions in the mantle wedge, causing the crust, including the pelagic sediment, to progressively dehydrate and release free H_2O or water. In our models, the free H_2O is stored and transported throughout the domain as a compositional field (Equation 4), that is, in addition to those representing crustal lithologies and serpentinite. Figure 2 shows a flowchart depicting the treatment of this water release, transport, and storage in the model. After the 0th timestep, mineral-bound H_2O is assigned in all source lithologies where water is expected to be present (i.e., following Figure 1b). At each subsequent timestep, the mineral-bound H_2O content for each lithology is recalculated using lookup tables created from Perple_X phase equilibria modeling results. This updated, mineral-bound H_2O content is then compared to the mineral-bound H_2O content of the previous step. If the new bound H_2O content is lower than the preceding timestep, then water must be released: the difference becomes the amount of the free H_2O phase present in the system that is produced by the metamorphic breakdown of hydrous minerals. If no H_2O release occurs, then no dehydration takes place.

STONER ET AL. 5 of 23

15252027, 2025, 11, Downloaded from https://agupubs.onlinelibrary.wiley.com/doi/10.1029/2025GC012488, Wiley Online Library on [16/11/2025]. See the Terms and Conditions

Figure 2. Flowchart illustrating our implementation of water release, transport, and storage. Bound H_2O is calculated using lookups created from the outputs of Perple_X phase equilibria calculations. At each timestep, new and old H_2O contents are calculated, and the remaining H_2O is transformed into a "free H_2O " phase, which percolates upward at 10 cm/yr. If free H_2O interacts with the mantle wedge it: (i) is absorbed into melts if the temperature is above the calculated wet solidus H_2O (Katz et al., 2003), (ii) continues to be advected upwards but causes a weakening of the surrounding mantle by 100x, if the temperature is between the temperature of the solidus and serpentinization, (iii) is bound within a "serpentinite field" if serpentinite is stable based on the associated lookup table.

Treating free H_2O and other lithologies as a continuum and not as particles means that in each model cell, the associated compositions can be less than unity, and hence individual compositions in the crustal column can numerically diffuse into each other (Kronbichler et al., 2012). During the dehydration calculations we therefore scale each bound H_2O amount for the magnitude of each composition (from 0% to 100%) within a given cell to prevent over or under-prediction of the H_2O content.

Free H_2O is, for simplicity, advected vertically upward at a constant rate of 10 cm/yr relative to the solid (e.g., Gerya et al., 2002; Gorczyk et al., 2007). In practice, this is implemented by modifying the ASPECT "plug-in" of Douglas et al. (2023) that adds two-phase (Darcy) flow to ASPECT. Here, instead of solving for the fluid velocity, we set the velocity at a constant value in the plug-in.

Free H_2O may interact with the mantle wedge in three ways: (a) if the temperature is above the calculated wet solidus (Katz et al., 2003), then all the free fluid is assumed to be absorbed into the melts, which can readily accept >10 wt. % H_2O (Gavrilenko et al., 2019; Hamilton et al., 1964; Mitchell et al., 2017). Melt migration and the effect of melt on viscosity are not modeled: a melt region is calculated purely to be consistent with H_2O being incorporated into melts, removing the associated free H_2O , and hence preventing extensive serpentinization of the base of the overriding plate in the "arc region;" (b) If the temperature is below that of the solidus yet above that of serpentinization stability, free H_2O continues to be advected upwards but weakens the surrounding mantle by a factor of 100. This mimics the weaker rheology of a hydrated peridotite, which has a lower viscosity than dry olivine aggregates as a proxy for peridotite (Hirth & Kohlstedt, 2003). (c) If the free H_2O is in the mantle and within the serpentinite stability field, it is bound within a "serpentinite compositional field." Free H_2O is not allowed to react with the overriding plate crust. Any free H_2O that reaches the Earth's surface is removed from the model.

Serpentinite can also be dragged downwards to P-T conditions outside serpentinite stability. While the resulting deserpentinization is not tracked directly, if any such material in the serpentinite field exits the region of serpentinite stability, then the background olivine flow law and peridotite density are re-imposed. For clarity, we use the terms "cumulative serpentinite" to denote the "serpentinite" compositional field, which includes both currently stable serpentinite and mantle material that has deserpentinized, and the term "instantaneous serpentinite," which refers to any serpentinite that is currently stable.

STONER ET AL. 6 of 23

2.3. Rheology

We first describe the overarching equations governing rheology, including yielding and creep deformation, within all model compositions. In subsequent subsections, we detail the parameters used for specific compositions. Overall, we adopt a composite flow law with diffusion creep, dislocation creep, and pseudo-plastic yielding (Glerum et al., 2018) for the background lithosphere and mantle (i.e., outside of the plate interface materials and any serpentinite). Both diffusion and dislocation creep mechanisms are assigned viscosities following the idealized flow law:

$$\eta_{\text{creep}} = A^{-\frac{1}{n}} \dot{\varepsilon}_{H}^{\frac{1-n}{n}} f_{\text{H}_2\text{O}}^r \exp\left(\frac{E_a + PV}{nRT}\right)$$
 (5)

where A is the creep prefactor, n is the stress exponent (1 for olivine diffusion creep; ~ 3.5 for olivine dislocation creep), $\dot{\epsilon}_H$ is the second invariant of the deviatoric strain rate, E is the activation energy, V is the activation volume, R is the ideal gas constant, and T is the temperature (Table 1). An exponential weakening term is also used for crustal rheologies whose P-T conditions intersect the solidus, which only occurs early in the model evolution (Figure S1 in Supporting Information S1). Despite the assumption of incompressibility in our conservation equations (Equations 1 and 2), we add a 0.3°C/km adiabatic temperature gradient to the temperatures used in the creep formulation.

We also incorporate pseudo-plastic yielding in the form of a "plastic" viscosity, η_{plastic} . The process of forming brittle fractures at the scale seen in nature, on the sub-meter scale or outcrop scale (e.g., Rowe et al., 2013), is computationally infeasible in the current models. Furthermore, multiple strain mechanisms, brittle, semi-brittle, and viscous may be operating concurrently. All such deformation processes tend to produce highly localized regions of shear in regions such as the bending portion of the subducting lithosphere (e.g., Ranero et al., 2003). We therefore subsume all such mechanisms into a plastic component using a 2-D Drucker-Prager criterion to prescribe a yield stress, σ_v :

$$\sigma_{v} = C\cos(\varphi) + \sin(\varphi)P \tag{6}$$

Where C is the cohesion, P the pressure, and φ is the friction angle. Furthermore, an array of studies has already shown that pore-fluid pressure along the subduction interface is likely high during shear (Audet & Bürgmann, 2014; Condit & French, 2022; Peacock et al., 2011). Therefore, we use an "effective friction" coefficient that is meant to encapsulate the effects of pore-fluid overpressure, which weakens the interface. We therefore recast Equation 6 as

$$\sigma_{v} = \mu_{\text{eff}} P + C_0 \tag{7}$$

$$\mu_{\text{eff}} = (1 - \lambda)\mu\tag{8}$$

Where C_o is a modified cohesion that includes the friction angle term, and λ is a pore fluid pressure coefficient. The plastic viscosity is then computed as a function of the yield stress and second invariant of the deviatoric strain rate:

$$\eta_{\text{plastic}} = \frac{\sigma_y}{2\dot{\epsilon}_{II}} \tag{9}$$

Viscosities associated with the different rheological mechanisms are then harmonically averaged to generate the model (or "composite") viscosity:

$$\frac{1}{\eta_{\text{composite}}} = \frac{1}{\eta_{\text{diff}}} + \frac{1}{\eta_{\text{disl}}} + \frac{1}{\eta_{\text{plastic}}}$$
(10)

The subscripts "diff," "disl," and "plastic" refer to diffusion creep, dislocation creep, and plastic viscosity components, respectively. If a model grid cell contains more than one composition (e.g., basalt and sediment), the

STONER ET AL. 7 of 23

respective composite viscosities are averaged using a geometric mean. All rheological parameters for all compositions are detailed in the following three sub-sections and listed in Table 1.

2.3.1. Mantle Rheology

The viscous component of the background mantle deforms via a combination of diffusion and dislocation creep, with activation volumes and energies corresponding to those of dry olivine (Karato & Wu, 1993; Table 1). Diffusion and dislocation prefactors are set to produce a composite viscosity of 2.5×10^{20} Pa s (i.e., $\eta_{\rm diff} = \eta_{\rm disl} = 5 \times 10^{20}$ Pa s) at a reference strain rate of 10^{-14} s⁻¹, the background mantle temperature, and lithostatic pressures corresponding to 330 km depth (cf. Billen & Hirth, 2005). These values result in sublithospheric deformation that is dominated by dislocation creep down to depths of ~250 km, which is broadly consistent with constraints from seismic anisotropy (Becker, 2006; Podolefsky et al., 2004). A weakening factor of $100\times$ is imposed in the mantle in regions with free H₂O to mimic the weaker rheology of hydrated peridotites (i.e., an additional 0.01 prefactor added to Equation 5), which have lower viscosities than the dry olivine used to approximate peridotite (Hirth & Kohlstedt, 2003).

At depths greater than 660 km, the lower mantle is allowed to deform only via diffusion creep, with the lower mantle diffusion creep prefactor set to produce a viscosity 20 times that of the upper mantle diffusion creep. The thickness of the transition to the lower mantle is 1 km. As outlined, our yield stress formulation considers both a friction coefficient μ , as traditionally measured in rock deformation experiments, and a pore fluid pressure factor to give an effective coefficient ($\mu_{\rm eff} = \mu(1 - \lambda)$; Equations 7 and 8). We set $\mu_{\rm eff} = 0.36$ (e.g., considering near-hydrostatic conditions with $\lambda = 0.4$ and $\mu = 0.6$) and a cohesion of 20 MPa (Table 1). At the trailing edges of the upper and subducting plates, we add a weak region to mechanically isolate the subducting and overriding plates from the adjacent thermal boundary layers that develop as the model evolves. These two weak regions are 30 km wide by 150 km deep with a constant yield stress of 1 MPa.

2.3.2. Crustal Rheology

For oceanic compositions, we use lookup tables (metabasalt, metagabbro) to impose the flow law associated with the weakest mineral predicted to be stable and hence dominate creep at those P-T conditions (Figure S1 in Supporting Information S1). In metamafic lithologies, dislocation creep flow laws are used for quartz (Hirth et al., 2001; as a stand-in for the blueschist facies glaucophane), amphibolite (Hacker & Christie, 1990), and eclogite (Zhang & Green, 2007). We adopt a dislocation creep quartz flow law for the pelagic sediments (Hirth et al., 2001). A maximum decoupling depth (MDD) of 200 km is chosen. That is, at depths greater than the MDD, the downgoing crust is assigned properties identical to the background mantle.

In terms of the plastic yield stress, we set the friction angle so that a $\mu_{\rm eff}$ of 0.36 is also used for metagabbro and upper plate crust (i.e., an equivalent yielding profile to that of the background mantle). We prescribe a low yield stress within the 145 km long initially curved portion of the interface ($\mu_{\rm eff} = 0.005$) to facilitate subduction initiation. A cohesion C_0 of 1 MPa is used for pelagic sediment and metabasalt and 20 MPa for metagabbro (Table 1; Equation 7).

2.3.3. Serpentinite Rheology

Modeled serpentinite deforms via the Peierls creep mechanism (low-temperature plasticity; Burdette & Hirth, 2022). Peierls creep is implemented as a dislocation creep approximation of the Peierls creep flow-law (Frost & Ashby, 1982; Kocks et al., 1975):

$$\dot{\varepsilon} = A\sigma^2 \exp\left(\frac{-Ea}{RT} \left(1 - \left(\frac{\sigma}{\tau_0}\right)^p\right)^q\right) \tag{11}$$

Where τ_0 is the low-temperature plasticity Peierls stress, σ the second invariant of the stress, p and q are empirical parameters, and E_a the activation energy for the Peierls mechanism. Unlike dislocation and diffusion creep (Equation 5), the Peierls creep flow law cannot be rearranged for stress because of the stress dependence in the exponent. Therefore, we use a dislocation creep-based approximation of low-temperature plasticity/Peierls creep (see Kameyama et al., 1999; Fildes & Billen, 2025; Text S1 in Supporting Information S1 for more details) with constants from Burdette and Hirth's (2022) antigorite experiments. At each time step, the stability field of

STONER ET AL. 8 of 23

15252027, 2025, 11, Downloaded from https://agupubs.onlinelibrary.wiley.com/doi/10.1029/2025GC012488, Wiley Online Library on [16/11/2025]. See the Terms

serpentinite is checked based on a lookup table, and if the composition is within serpentinite stability, the full Peierls creep flow law is used for model cells above 10 wt. % serpentinite (Escartín et al., 2001). In regions below 10 wt. % serpentinite, the serpentinite rheology is geometrically averaged along with the other composition(s) in the cell. Viscosity is thus reduced in regions where serpentinite exceeds the threshold. Outside of serpentinite stability, we adopt the olivine rheology imposed on the background mantle. Water that would be re-released by deserpentinizing material is not tracked.

We also include a plastic yielding component in the serpentinite rheology. Reported serpentinite yield stresses span a broad range of values depending on serpentine species, temperature, velocity, and pressure. For example, reported friction coefficients (μ) of lizardite range from 0.18 (Carpenter et al., 2009; Tesei et al., 2018) to ~0.55 (Dengo & Logan, 1981; Moore et al., 1997), with many experiments falling in the 0.25–0.4 range (Behnsen & Faulkner, 2012; Moore & Lockner, 2004; Scuderi & Carpenter, 2022). Conversely, antigorite (the high temperature polymorph of serpentinite), generally has a higher coefficient of friction of 0.5–0.85 (Raleigh & Paterson, 1965; Reinen et al., 1994), which may be decreased if dissolution-precipitation creep enhances susceptibility to failure (Behr & Platt, 2013; Rutter, 1976; Tulley et al., 2024). Given this uncertainty, we explore a range of values for the serpentinite yield strength, with $\mu_{\rm eff}$ = 0.01–0.04 and a cohesion of 1 MPa (i.e., considering $\lambda \sim 0.90$ –0.95 and μ = 0.2–0.6; Table 1). We provide more detailed discussion and references on both the Peierls creep formulation and serpentinite yielding in Supporting Information S1 (Text S1).

3. Results

We first present our reference subduction model that includes serpentinite ingrowth over time. Next, we analyze similar models with variable H_2O inputs into the subduction zone, including with and without a sediment layer. Finally, we vary serpentinite strength to test the sensitivity of subduction kinematics and slab P-T conditions to our rheological assumptions about the weak, accumulating serpentinite along the plate interface.

To ensure consistency in comparing serpentinite ingrowth across simulations, we compare model snapshots at timesteps with equivalent total amounts of subducted plate length (i.e., net convergence) and therefore equivalent amounts of net bound $\rm H_2O$ input from the portion of the downgoing slab beneath the variably hydrated sediment layer. We focus on timesteps at which the net convergence corresponds to approximately that required for the downgoing plate to reach the lower mantle (i.e., net convergence ~ 860 km). For completeness, we also present comparisons at equivalent model times in Supporting Information S1 (Figure S3) as well as additional tests that individually exclude various complexities from the reference models, namely serpentinite, fluid-induced mantle weakening, and the use of phase diagram lookups to derive the density and viscosities of the interface/crustal lithologies (Figures S4–S7 in Supporting Information S1).

3.1. Reference Model

Because the models are dynamic, plate motions are not imposed and hence subduction geometries and velocities evolve freely through time, thereby impacting, and being impacted by serpentinite ingrowth for 50 Myr (Figure 3). The co-evolving convergence rates, serpentinite content, and slab P-T profiles are displayed in Figure 4 for the reference model. The P-T profiles are overlain on the pseudosections used for pelagic sediment and metabasalt (Figures 4b and 4c), the two most hydrated lithologies of our model slab.

During the subduction infancy stage (I), until \sim 8 Myr, the slab largely sinks near-vertically (Figure 3a). Subduction is relatively sluggish but accelerates from \sim 3 to 5.5 cm/yr (Figure 4a). Convergence is dominantly accommodated via rollback, with overriding plate motion initially \sim 5× faster than that of the subducting plate. This infancy stage is the hottest phase, with a slabtop significantly warmer than during the latter stages (Figure 4b). As a result, H_2O is released from the downgoing oceanic crust into the mantle wedge only down to a maximum depth of \sim 60 km at 0.7 Myr (Figure 3a). Released H_2O migrates upwards until it either: (a) enters a region where melt is stable, where it is removed or (b) enters a region where serpentinite is stable, where it is bound in serpentinite in the mantle wedge (Figure 3c). During this initiation phase, serpentinite formed and dragged down over the total model run—cumulative serpentinite—is approximately equal to the instantaneous serpentinite—the amount of stable serpentinite in the mantle wedge at any given point in time. That is, there is minimal downdragging of serpentinite during the initiation stage. Additionally, there is relatively modest serpentinite production: Only <20% of cumulative serpentinization of the entire model duration is produced by the end of this phase (Figure 4a). At the beginning of this stage (0.7 Myr), the amount of serpentinite has not yet

STONER ET AL. 9 of 23

15252027, 2025, 11, Downloaded from https://agupubs.onlinelibrary.viley.com/doi/10.1029/2025GC012488, Wiley Online Library on [16/11/2025]. See the Terms and Conditions (https://onlinelibrary.viley.com/terms-and-conditions) on Wiley Online Library for rules of use; OA articles are governed by the applicable Creative Commons Licensia

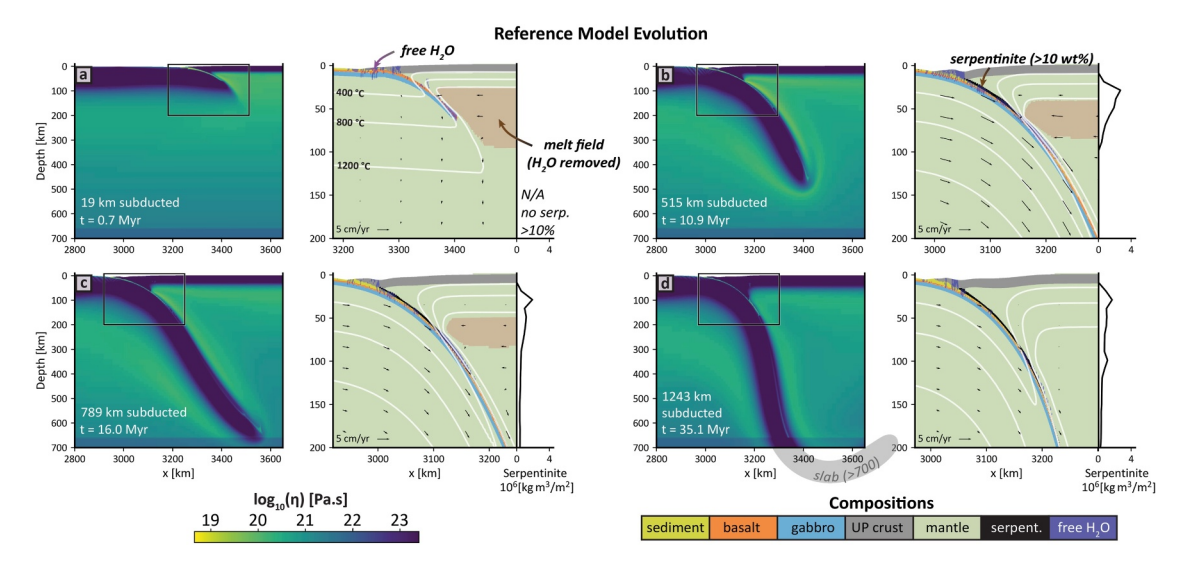


Figure 3. Snapshots of reference model evolution. (a), (b) Model stages showing the initiation (Phase I) and free-sinking phases (Phase II), respectively, with the downgoing slab releasing free H₂O that hydrates the mantle wedge via serpentinization ("cumulative serpentinization" shown). (c), (d) Evolution just before (Phase II) and after (Phase III) the core of the slab passes the 660 km deep transition zone. (d) Gray shows extent of slab outside zoom-in region. To limit excess hydration of the overriding plate, a hydrous "melt" region is calculated (Katz et al., 2003), where free H₂O is assumed to be incorporated into melt and removed from the system (see Methods, Section 2.2, for details).

exceeded the 10 wt. % serpentinite per cell threshold that triggers the full weak serpentinite rheology (Figure 3a), and therefore the accelerating convergence rate is not due to serpentinite ingrowth, creating a layer 5 km thick (Figure S8 in Supporting Information S1).

During the following free sinking phase (II), the tip of the downgoing plate approaches the 660 km transition at a steep dip (Figure 3b) before flattening out to a sub-horizontal angle (Figure 3c). At this point, the convergence rate reaches its maximum value (Figure 4a), and both these higher advection rates of the sinking slab and thickening of the cold forearc region (i.e., an increase in the "decoupling depth") cause temperatures to cool by ~200°C at 3 GPa from 10.9 to 16.0 Myr. Such cooling has been seen in previous time-dependent subduction models (Holt & Condit, 2021; Kincaid & Sacks, 1997; Turino & Holt, 2024; Wang et al., 1995). As a result of cooler temperatures, water release from the oceanic crust occurs at greater depths than during subduction infancy, down to 80 km (Figure 4c). However, water release in pelagic sediments has a shallow pulse at ~30 km that coincides with the depths of dehydration from the loss of stilpnomelane (Figure S9 in Supporting Information S1). Mantle wedge

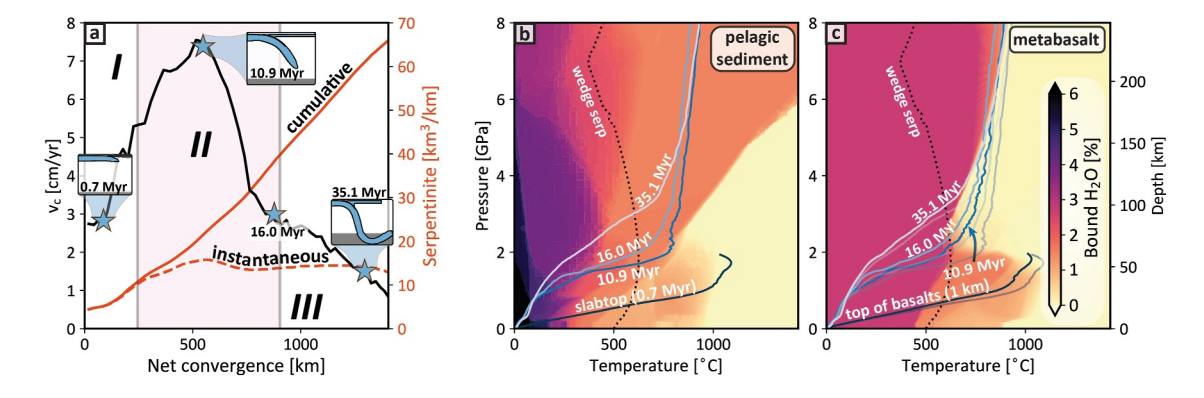


Figure 4. Kinematic and thermal evolution of the reference model. (a) Ingrowth of cumulative serpentinite produced over the course of the model, and instantaneous serpentinite content including serpentinite stable at a given point in time, that is, without deserpentinized/downdragged material. I refers to the infancy stage, II to the free sinking phase, III to the mature phase as classified by previous studies (e.g., Holt & Condit, 2021). (b) Evolution of slabtop and (c) near slabtop thermal states. Background shows bound water used in lookups for pelagic sediments and metabasalts, respectively. Serpentine stability in the mantle wedge is also shown for reference. Lightly shaded pressure-temperature (P-T) paths (c) coincide with the slabtop P-T, and darker shading coincides with P-T conditions at the top of the metabasalt section, 1 km deep normal to the plate interface.

STONER ET AL. 10 of 23

15252027, 2025, 11, Downloaded from https://agupubs.onlinelibrary.wiley.com/doi/10.1029/2025GC012488, Wiley Online Library on [16/11/2025]. See the Terms and Conditions

and-conditions) on Wiley Online Library for rules of use; OA articles are governed by the applicable Creative Co

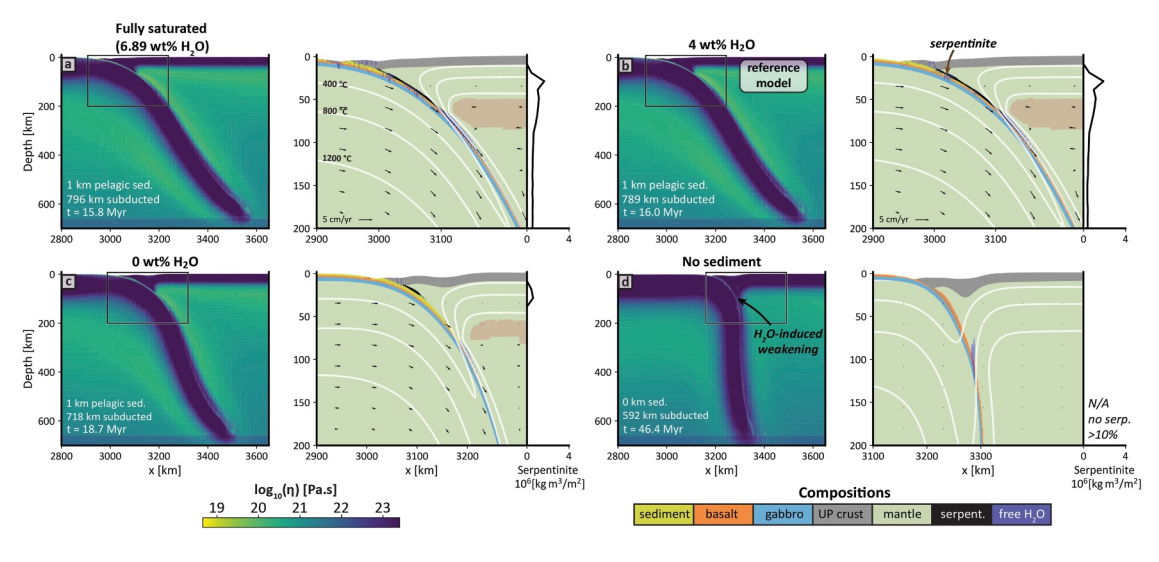


Figure 5. Snapshots of models while varying the hydration state of the incoming sediment. To standardize the amount of bound water input into the subduction zone, all model time slices are shown for the same distance subducted, approximately enough to reach the 660 km transition zone. (a–c) Models showing variation in sediment hydration state from fully hydrated to anhydrous (6.89%–0%). (d) No sediment but with other lithologies (metabasalt, metagabbro) still initially hydrated.

serpentinite content is greatest shallower than 50 km (1.7 GPa) depth, approximately where these pelagic sediments dehydrate, while deeper dehydration arises from the dehydrating oceanic section (Figures 4b and 4c). Water released by slab dehydration causes more serpentinite to accumulate in the mantle wedge, increasing instantaneous serpentinite content by ~40% over phase II from ~12 km³/km to a peak of ~16 km³/km. During this phase, serpentinite also begins to be dragged downwards to P-T conditions where serpentine is unstable and thus breaks down; hence, instantaneous serpentinite (stable in the interface/forearc) becomes significantly less than cumulative serpentinite. Therefore, during this stage, downdragging begins to exceed serpentinite ingrowth, causing the amount of instantaneous serpentinite in the mantle wedge to start to decrease (Figure 4a). However, throughout this phase, and in contrast to the earlier phase, enough serpentinite has accumulated to exceed the 10 wt. % serpentinite lubrication threshold along the interface, and therefore the plate interface is lubricated by serpentinite (Figures 3b and 3c).

The sinking of the slab into the lower mantle, past the 660 km transition zone, marks the beginning of the mature phase (III; Figure 3d). After ~17.6 Myr (the boundary between phase II and III), convergence rates decrease to below 2 cm/yr; this slowdown is driven by the slab penetrating the high viscosity lower mantle. Slab P-T conditions are too cold for metabasalts and metagabbros to dehydrate within the serpentinite field, and any additional dehydration must come from metasediments (Figure 4b). Dehydration of metasediments continues, causing the cumulative serpentinite to progressively increase. However, most newly formed serpentinite is dragged downwards (Figure 3d). In fact, downdragging slightly outpaces ingrowth, causing instantaneous serpentinite to decrease ~5% from 17.6 to 50 Myr (Figure 4a).

3.2. Variable H₂O Input

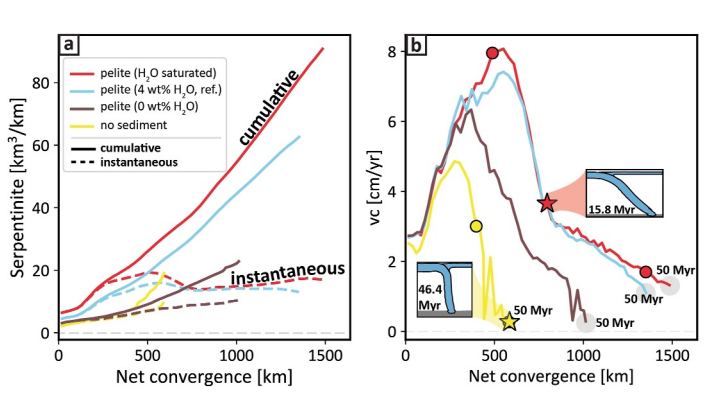
To examine the effect of mineral-bound H_2O content on slab dehydration and forearc serpentinization, we vary water content in the downgoing 1-km-thick sediment layer, comparing a "fully saturated" case with the maximum amount of mineral-bound H_2O (6.89 wt. %), our intermediate, moderately hydrated reference case (4 wt. % H_2O), and a completely anhydrous case with 0% H_2O (Figures 5a–5c). Additionally, we include a limiting case identical to those shown in Figures 5a–5c but with no sediment layer above the metabasalts (Figure 5d). In both the anhydrous and no-sediment cases, H_2O is released exclusively from the metabasalts and metagabbros.

Incoming plates with different amounts of incoming bound water subsequently release variable amounts of water that migrate to the mantle wedge to produce serpentinite. The greatest amounts of serpentinite are produced in the fully saturated case, both for total cumulative serpentinite, which includes deserpentinized material, and instantaneous serpentinite. In the fully saturated case, there is therefore the most serpentinite available to lubricate the interface (Figure 5a). The fully saturated and moderately hydrated cases both produce more serpentinite than

STONER ET AL. 11 of 23

15252027, 2025, 11, Downloaded from https://agupubs.onlinelibrary.wiley.com/doi/10.1029/2025GC012488, Wiley Online Library on [16/11/2025]. See the Terms and Conditions (https://onlinelibrary.wiley.com/terms

-and-conditions) on Wiley Online Library for rules of use; OA articles are governed by the applicable Creative Commons Licenso



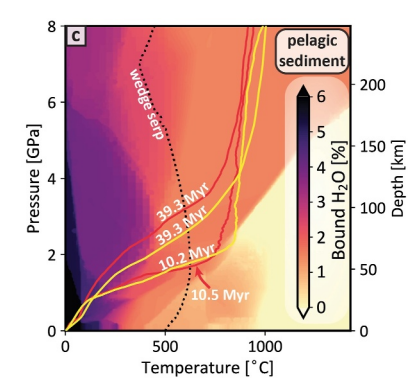


Figure 6. Kinematic and thermal evolution of models with varying water content in sediment or without sediment. (a) Ingrowth of serpentinite over the course of the model run, either considering the cumulative serpentinite that includes both stable serpentinite and deserpentinized material or the instantaneous amount that only includes the amount of serpentinite that is stable. (b) Plate convergence rates for different models. Filled circles denote times when slabtop pressure-temperature (P-T) conditions are plotted in c. (c) Slab P-T profiles at two model timesteps for the fully saturated and no sediment cases overlain on the pseudosection for pelagic sediment.

the anhydrous case and the case without a sediment layer. The fully saturated and moderately saturated cases also reach a quasi-steady state, but the anhydrous (0 wt. %) case and case without sediment do not (Figure 6a).

In the case without a sediment layer, there is no sediment to insulate the metabasalt layer at the interface, and so the hydrated metabasalts are directly exposed to the hotter temperatures in the mantle wedge (Figure S10 in Supporting Information S1). As a result, the metabasalts are hotter and dehydrate more completely, and more cumulative serpentinite is produced in this model than within the anhydrous case. This case without a sediment layer, however, drags down more serpentinite, which acts to reduce the volume of stable instantaneous serpentinite in the wedge to levels comparable to the case with a sediment layer. There is more downdragging because the rheology of metabasalts of the oceanic crust follows a strong eclogite flow law above ~ 1.5 GPa (i.e., $\eta_{\text{eclogite}} >> \eta_{\text{antigorite}}$), whereas the rheology of sediments is governed by a weaker quartz flow law.

As seen in previous numerical subduction models (e.g., Behr et al., 2022; Čížková & Bina, 2013), a weaker plate interface results in faster convergence rates. However, in this suite of models, variations in the effective plate interface strength result from varying volumes of weak serpentinite. During subduction infancy, serpentinite begins to accumulate but not in sufficient volumes to exert a lubricating effect; the convergence rates in all models evolve similarly and accelerate, although the case without sediment is ~0.5 cm/yr slower at the start of the model because there is no sediment to weaken the interface (Figure 6b). After the initiation stage, the case with the most incoming water has the highest degree of serpentinite production and experiences the fastest convergence rates (~8 cm/yr), whereas the anhydrous case reaches maximum convergence rates of ~6 cm/yr. Cases with no pelagic sediment only reach a maximum convergence rate of ~5 cm/yr and become locked by the end of the model run (Figure 6b). This locking coincides with an increase of the interface viscosity by approximately two orders of magnitude (Figure S8 in Supporting Information S1) because serpentinite accumulation that could weaken the interface is relatively low (Figure 5). The variation in slab dip is also linked to differences in the amount of water released and serpentinite formed (Figures 5 and 6a). As the slab without sediment reaches the highly viscous 660 km transition zone, and convergence rates slow to <1 cm/yr, the dip increases dramatically. Therefore, the ingrowth of weak serpentinite produces slabs with higher convergence rates and shallower dips, whereas the case with no water has more downdragging of serpentinite, lower convergence rates, and higher dips.

Thermal state is, in turn, linked to subduction kinematics. The models with faster convergence rates, due to greater serpentinite volumes and therefore a weaker interface, have a cooler slabtop due to more rapid downward advection of the cold lithospheric plate. In contrast, the case without sediment and with slow convergence has a warmer slabtop (Figure 6c) due to feedback between serpentinization, interface strength, and convergence rate.

3.3. Variable Yield Strength

Finally, we test the effect of serpentinite yield strength on model evolution, with snapshots of the slab morphology for models with serpentinite strength again plotted for equivalent net plate convergence (Figure 7). We vary yield

STONER ET AL. 12 of 23

1525/2027, 2025, 11, Downloaded from https://agupubs.onlinelibrary.wiley.com/doi/10.1029/2025GC012488, Wiley Online Library on [16/11/2025]. See the Terms and Conditions (https://onlinelibrary.wiley.com/erms-and-conditions) on Wiley Online Library for rules of use; OA

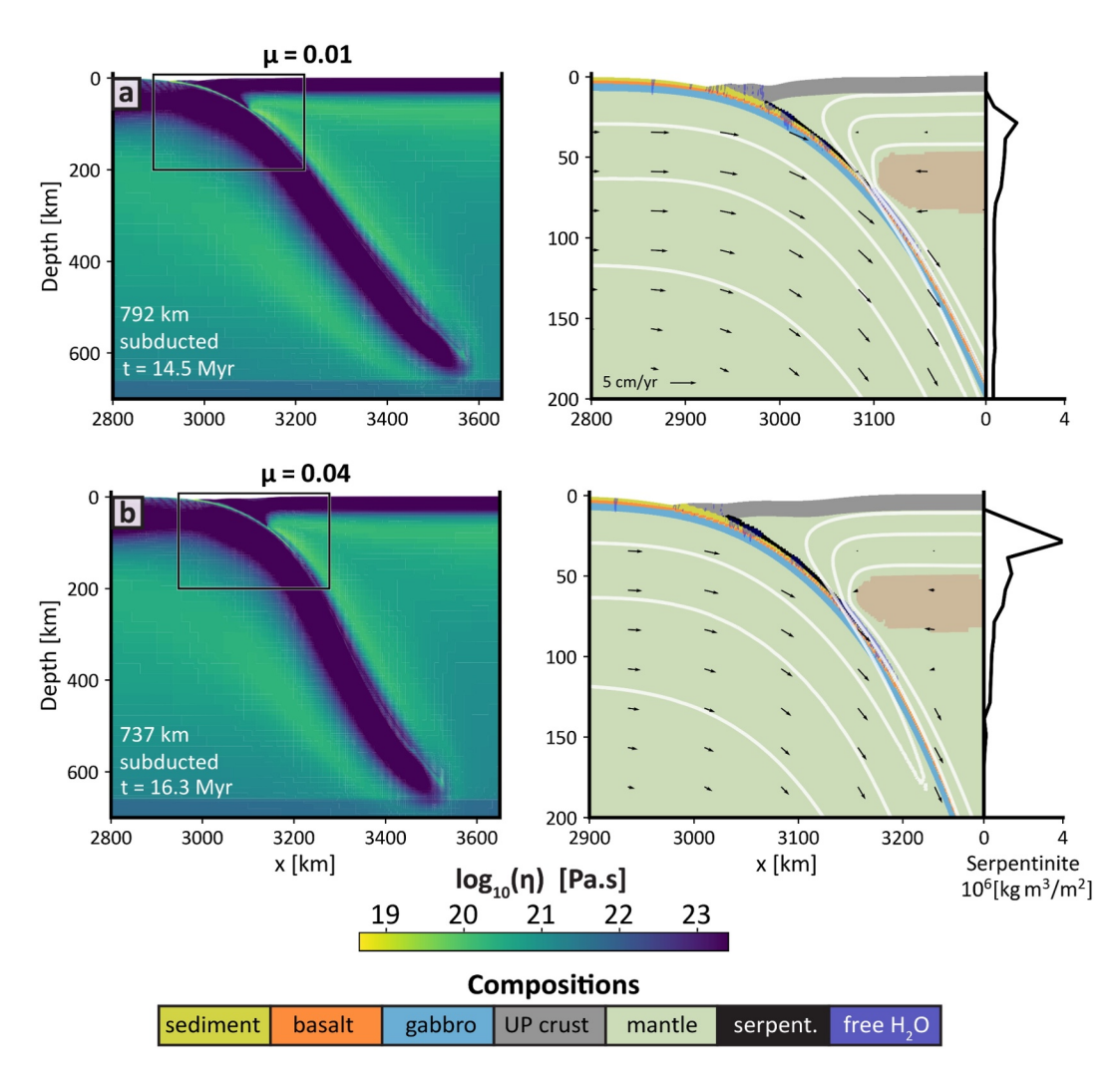


Figure 7. Snapshots of the subducting plate as a function of friction parameters in serpentinite with all other parameters identical to the reference model are shown in Figure 3: (a) a low frictional strength case; (b) a high frictional strength case. All cases are plotted at the same time step, approximately the time for the subducting plate to reach the transition zone.

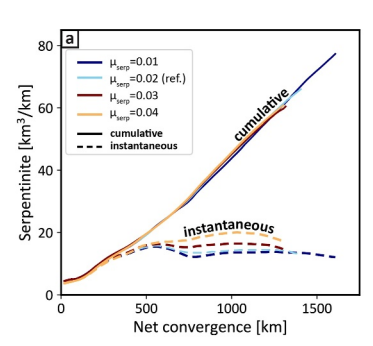
strength values by adjusting the effective coefficient of friction $\mu_{\rm eff}$ from 0.01 to 0.04 above and below the reference value of 0.02 (Equation 7).

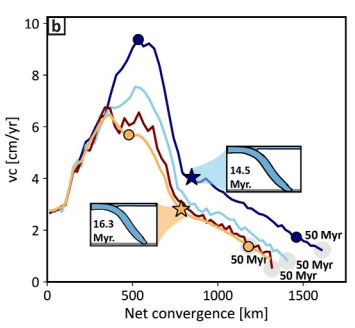
The cumulative amount of serpentinite created over the entire model duration is approximately equivalent for any amount of convergence regardless of serpentinite strength (Figure 8a). However, different serpentinite strengths lead to different degrees of downdragging that impact both the instantaneous serpentinite amounts and hence convergence rates over time. During the initiation stage (slab depths <400 km), all models evolve similarly, with little variation in the downdragging of serpentinite (Figures 8a and 8b). However, after the initiation stage, serpentinite retention is very sensitive to serpentinite strength: weak forearc serpentinites with low friction coefficients are dragged down more easily than those with high friction coefficients, despite similar cumulative serpentinite ingrowth. That is, the serpentinite stable at any given time—the instantaneous serpentinite—is affected by downdragging. At the end of the free sinking phase there is ~40% more instantaneous serpentinite in the high friction case ($\mu_{\rm eff} = 0.04$) compared to the case with the weakest yielding parameters ($\mu_{\rm eff} = 0.01$; Figure 7). An even higher friction coefficient of 0.06 was separately tested and, in line with this trend, resulted in the most serpentinite retention and the least downdragging (Figure S11 in Supporting Information S1).

These differences in serpentinite strength and hence retention and downdragging are linked to changes in kinematics and thermal state. The case with the lowest serpentinite strength reaches maximum convergence rates of nearly 9.4 cm/yr, whereas the strongest case plotted has maximum convergence rates that are lower by 30%

STONER ET AL. 13 of 23

1525207, 2025, 11, Downloaded from https://agupubs.onlinelibary.wiley.com/doi/10.1029/2025GC012488, Wiley Online Library on [16/11/2025]. See the Terms and Conditions (https://onlinelibary.wiley.com/terms-and-conditions) on Wiley Online Library for rules of use; OA articles are governed by the applicable Creative Commons Licenses





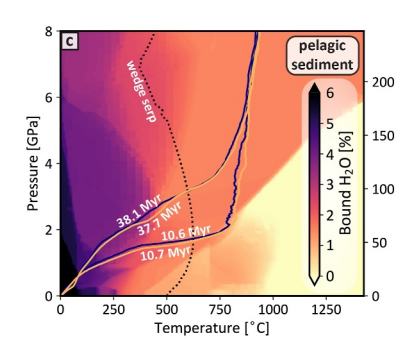


Figure 8. Kinematic and thermal evolution of models with variable effective friction coefficient of serpentinite. (a) Ingrowth of serpentinite over the course of the model run, either considering the cumulative serpentinite amount that was created over the duration of the entire model run or the instantaneous amount that indicates the amount of serpentinite that is stable at any given point in time. The difference between the two is an indication of the degree of loss of serpentinite due to coupling with the downgoing plate. (b) Changes in convergence rate for different models as a function of serpentinite strength. Filled circles denote times when slabtop pressure-temperature conditions are plotted in c. (c) The thermal state at two snapshots in time for the strongest and weakest plotted endmembers of serpentinite strength.

(Figure 8b). Therefore, even though there is more instantaneous serpentinite in the wedge in the high strength case, it is the high strength of serpentinite, not the abundance, that exerts a larger influence on kinematics and produces the lower convergence rates. Finally, the lower convergence rates in the higher strength case produce warmer slab P-T conditions (Figure 8c) because the slab experiences more diffusive heating from the overlying mantle wedge. This difference in temperature does not lead to a significant difference in cumulative serpentinite production because the slab P-T conditions still pass through the same dehydration reactions (Figure 8c).

4. Discussion

4.1. Ingrowth of Serpentinite

Despite exerting a critical influence on magmatism, seismicity, and the exhumation of rocks from depth, the mantle wedge remains one of the most enigmatic regions of the subduction system. In particular, the amount of water bound in hydrous minerals, particularly serpentinite, is poorly resolved, partly due to the paucity of phase changes in wedge serpentinites, which complicates efforts to precisely constrain P-T conditions experienced by those rocks. Unlike many crustal rocks, serpentinites rarely contain minerals suitable for geochronology. Consequently, constraining the ingrowth of serpentinites in the mantle wedge as well as linking them to large-scale subduction evolution necessitates alternative approaches, such as geochemical analyses of arc magmas or serpentinite mud volcanoes, geophysical techniques, and numerical modeling (e.g., Abers et al., 2017; Fryer et al., 1999; Hyndman & Peacock, 2003; Tatsumi, 1986; Tatsumi & Eggins, 1995). Linking mineral phase stability calculations in the downgoing plate to thermomechanical models provides a quantitative framework for evaluating serpentinite stability and the amount of water released by the slab. Our numerical models expand on this framework by integrating the thermal state of the downgoing slab to its dewatering processes, the resulting mantle wedge hydration over time, and subsequent rheological transformations, thereby complementing petrological and geochemical techniques (e.g., Scambelluri & Tonarini, 2012).

This work examines the effects of the progressive ingrowth and buildup of serpentinite in the mantle wedge over the lifetime of a subduction zone (Figures 4–8) within dynamic models that implicitly contain feedback between thermal structure, dehydration, serpentinite accumulation, and resultant interface strength changes. Extensive geodynamic and petrological modeling has shown that water released from the downgoing slab hydrates and serpentinizes the forearc mantle wedge (e.g., Abers et al., 2017; Condit et al., 2020; Peacock, 1987; Wada & Wang, 2009). These studies have successfully tracked serpentinization in the context of exhumation, wedge dynamics, magmatism, and/or decoupling of the downgoing slab from the overriding wedge (Arcay et al., 2005; Gerya et al., 2002; Gerya & Meilick, 2011; Kerswell et al., 2021; Li et al., 2019; Nikolaeva et al., 2008). Previous work has already examined some feedback caused by serpentinization. For instance, rapid serpentinization during subduction infancy has been linked to evolving temperatures in the slab (Epstein et al., 2024), and interface strength has been shown to modulate both force balances (Arcay et al., 2005; Gerya et al., 2008; Lamb & Davis, 2003) and plate convergence rates (Behr & Becker, 2018; Behr et al., 2022; Conrad & Hager, 1999). However, how the time-dependent ingrowth of serpentinites, and thus the development of a weak interface, feed

STONER ET AL. 14 of 23

15252027, 2025, 11, Downloaded from https://agupubs.onlinelibrary.wiley.com/doi/10.1029/2025GC012488, Wiley Online Library on [16/11/2025]. See the Terms and Conditions

back into subduction kinematics, such as plate velocities and slab morphology, was beyond the scope of most previous studies. A select few studies, however, use dynamic numerical models to explore the impact of mantle hydration-induced weakening on subduction, but with a weakening and density parameterization not specific to serpentinization (Douglas et al., 2025; Nakao et al., 2016, 2018; Ritter et al., 2024). These studies revealed feedback between large-scale kinematics and hydration-induced weakening of the mantle wedge, a result confirmed by our work, as well as convergence rate slowdowns associated with buoyancy from abyssal hydration of the downgoing plate. Apart from the above, such feedbacks are rarely incorporated in detail into dynamic and time-dependent subduction modeling studies. Instead, many studies typically impose kinematic boundary conditions—usually plate velocities—and hence prevent the progressively accumulating weak serpentinite from influencing large-scale plate motions. In contrast, our dynamic models allow plates to evolve freely, capturing key feedback between serpentinite rheology, mantle wedge hydration, and thermal state.

The extent of serpentinization of the mantle wedge over time is a mass balance between serpentinite ingrowth and loss. Ingrowth of mantle wedge serpentinite depends on the amount of water released from the downgoing slab, depending on the thermal state. From the exhumed rock record, slabs are predicted to be warmest during the earliest phases of subduction, after which they cool down (Agard et al., 2018; Cloos, 1985; Penniston-Dorland et al., 2025; Platt, 1975). In dynamic subduction models, such as those presented herein, this thermal evolution emerges as both slab sinking accelerates and the base of the cold forearc (i.e., the "decoupling depth") migrates to greater depths above the slab (Figures 3 and 4; cf. Holt & Condit, 2021). Recent work shows that this time-evolving thermal structure exerts a significant impact on predictions of slab dehydration and mantle forearc serpentinization (Epstein et al., 2024). Our work finds similar results: initial rates of serpentinization are fastest during the hot early stages, when the slab can fully dehydrate, and before significant volumes of serpentinite have begun to be dragged down into the deeper mantle.

Serpentinite ingrowth is also strongly influenced by the composition of the downgoing material that uniquely responds to the P-T conditions it encounters. Hydrated sediment produces more water that drives serpentinization in the mantle wedge compared with metagabbros and metabasalts (Figure 5). More serpentinization in sediment-rich models was originally shown for a sediment with an averaged sediment composition (GLOSS), which also tends to dehydrate at shallower conditions than metabasalts (Rüpke et al., 2004). Greater serpentinization extents with more sediment are also consistent with more recent modeling (Abers et al., 2017; Epstein et al., 2024). Models without sediment result in less mantle wedge serpentinization because the package of subducting metabasalts on average contain less water than pelagic sediment (2.3 wt.% vs. 6.89 wt.%) and dehydrate at P-T conditions outside those of serpentine stability, particularly as the model matures (Figures 5 and 6). Although other siliciclastic sediment compositions may exhibit different dehydration patterns, a global assessment of the most common subducting sediment compositions (Plank & Langmuir, 1998) finds pelagic sediments to be the most prevalent. Non-siliciclastic compositions, such as carbonate-rich sediments, undergo devolatilization to produce complex, mixed-volatile fluids, which may further weaken the plate interface (Oyanagi & Okamoto, 2024), but decarbonation and consideration of high-solute fluids is beyond the scope of the current work.

Downdragging represents an additional complexity by removing previously accumulated serpentinite from the mantle wedge. Significant coupling between serpentinite and the downgoing slab was originally proposed as a mechanism to delay dehydration of material in or near the slab until it reaches depths necessary for generating hydrous arc magmas (Tatsumi, 1986). This is also evidenced geochemically by the striking similarity between forearc serpentinites and arc magmas (Scambelluri et al., 2019; Tonarini et al., 2011). From a mass balance perspective, downdragging would prevent some forearcs from being oversaturated (Abers et al., 2017; Epstein et al., 2024; Savov et al., 2007). However, the balance between coupling and downdragging has largely been modeled in the context of subduction erosion (Angiboust et al., 2012), the formation of a subduction channel (Gerya et al., 2002; Gerya & Meilick, 2011; Hilairet & Reynard, 2009; Schwartz et al., 2001), and downdragging of water bound in the mantle (Nakao et al., 2016, 2018). While we only consider a limited range of serpentinite strengths in our time-dependent models (Figure 7), our results agree with more extensive targeted modeling demonstrating that serpentinite downdragging depends on serpentinite rheology (Douglas et al., 2023). We find that cases with low effective friction coefficients (0.01) have $\sim 2 \times$ more cumulative serpentinite than is currently stable as instantaneous serpentinite, while the high friction case (0.04) has only ~35% more cumulative serpentinite (values extracted at the timesteps with maximum convergence rates). Nonetheless, a rheologically weak layer of serpentinite ~5 km thick above the downgoing slab forms and stabilizes within our models with sediment,

STONER ET AL. 15 of 23

15252027, 2025, 11, Downloaded from https://agupubs.onlinelibrary.wiley.com/doi/10.1029/2025GC012488, Wiley Online Library on [16/11/2025]. See the Terms and Conditions (https://onlinelibrary.wiley.com/doi/10.1029/2025GC012488, Wiley Online Library on [16/11/2025]. See the Terms and Conditions (https://onlinelibrary.wiley.com/doi/10.1029/2025GC012488, Wiley Online Library on [16/11/2025]. See the Terms and Conditions (https://onlinelibrary.wiley.com/doi/10.1029/2025GC012488, Wiley Online Library on [16/11/2025]. See the Terms and Conditions (https://onlinelibrary.wiley.com/doi/10.1029/2025GC012488, Wiley Online Library on [16/11/2025]. See the Terms and Conditions (https://onlinelibrary.wiley.com/doi/10.1029/2025GC012488, Wiley Online Library on [16/11/2025]. See the Terms and Conditions (https://onlinelibrary.wiley.com/doi/10.1029/2025GC012488, Wiley Online Library on [16/11/2025]. See the Terms and Conditions (https://onlinelibrary.wiley.com/doi/10.1029/2025GC012488, Wiley Online Library on [16/11/2025]. See the Terms and Conditions (https://onlinelibrary.wiley.com/doi/10.1029/2025GC012488, Wiley Online Library on [16/11/2025]. See the Terms and Conditions (https://onlinelibrary.wiley.com/doi/10.1029/2025GC012488, Wiley Online Library on [16/11/2025]. See the Terms and Conditions (https://onlinelibrary.wiley.com/doi/10.1029/2025GC012488, Wiley Online Library.wiley.com/doi/10.1029/2025GC012488, Wiley Online Library.wiley.com/doi/10.1029/2025GC012488,

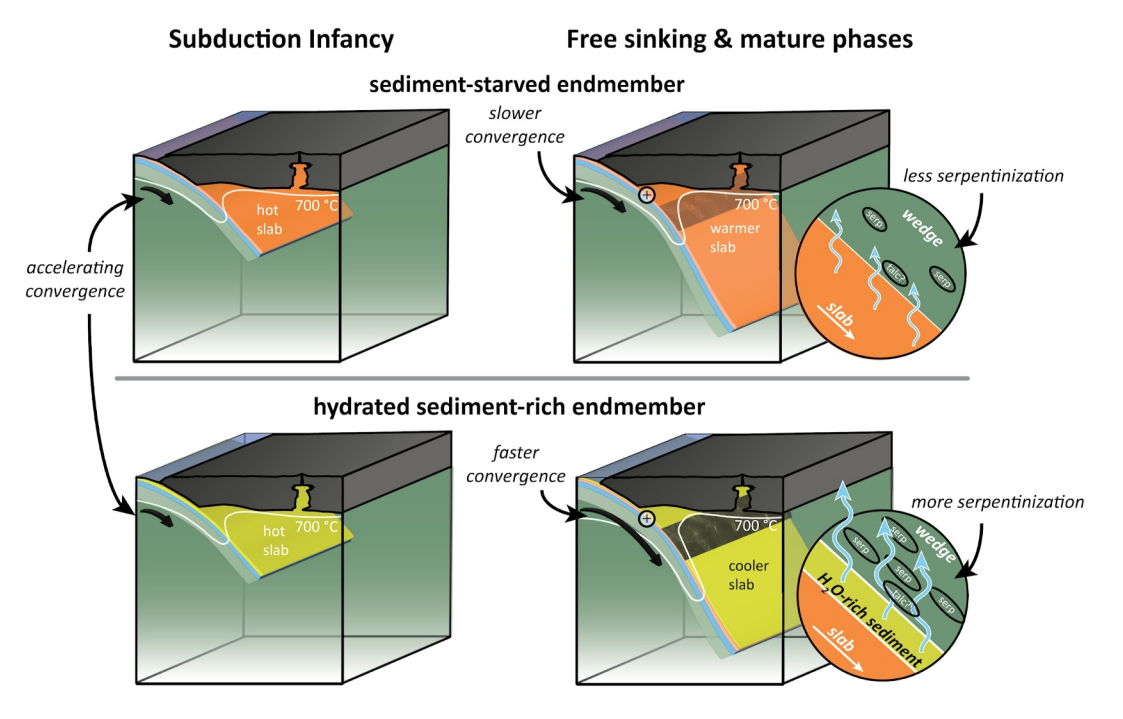


Figure 9. Summary of evolutionary feedback in our numerical results. The ingrowth of serpentinite reduces shear stress along the plate interface changing plate convergence rates, which in turn can change the thermal state over time. All three processes are interconnected and can accentuate the influence of weak, hydrated subducting lithologies, such as sediment, on plate speeds. Shaded regions in the free sinking/mature phase correspond to regions of active serpentinization.

which is broadly consistent with, for example, recent seismological estimates using receiver functions in Cascadia (Figure S8 in Supporting Information S1; Audet et al., 2025).

4.2. Effects of Serpentinite Ingrowth on Plate Kinematics

The potential link between slab fluid release, interface strength, and hence, subducting plate deformation was first recognized during the plate tectonics revolution. Studies noted that mineralogically bound volatiles would be liberated during subduction and weaken the plate interface (Isacks et al., 1968; Isacks & Molnar, 1971). A weakening of the interface affects the stress state along the interface and thus the overall subduction zone force balance over both long and short timescales (e.g., Behr & Becker, 2018; Conrad & Hager, 1999; Julve et al., 2024; King & Hager, 1990; Moreno et al., 2014).

An array of processes may lubricate the plate interface, thereby reducing interface shear resistance, and, in turn, elevating plate speeds. In particular, the interface may be lubricated by sediment or ingrowing serpentinite. However, unlike sediment (Behr et al., 2022; Lamb, 2006; Pusok et al., 2022) or mantle wedge hydration (Arcay et al., 2005; Gerya & Meilick, 2011; Nakao et al., 2016, 2018; Ritter et al., 2024; Wada & Wang, 2009), the direct impact of interface/wedge serpentinization on plate evolution has rarely been explicitly examined in fully dynamic models. In our models, serpentinite accumulation elevates convergence rates after subduction infancy as, during the earliest phase, weak serpentinite has not yet accumulated to sufficient degrees to significantly reduce the interface stress state. However, during the following free-sinking phase, greater volumes of weak serpentinite have accumulated, causing reduced shear stresses along the interface and thus faster convergence rates (Figure 5). Therefore, in our models, sediments weaken the interface by both reducing the in situ strength of the interface, as previously shown, and by releasing water and further weakening the interface via the progressive formation of weak serpentinite. Instantaneous serpentinite increases by 20%—40% during the mature and free sinking phases compared to subduction infancy, and so the associated convergence rate increase is similarly time dependent (Figure 9).

A weaker interface has also been linked to the formation of a subduction channel (Shreve & Cloos, 1986), which, when dominated by buoyant serpentinite, may aid the exhumation of negatively buoyant lithologies, such as

STONER ET AL. 16 of 23

15252027, 2025, 11, Downloaded from https://agupubs.onlinelibrary.wiley.com/doi/10.1029/2025GC012488, Wiley Online Library on [16/11/2025]. See the Terms and Conditional Cond

eclogites, from mantle depths (e.g., Gerya et al., 2002; Schwartz et al., 2001). Because we find time-dependent ingrowth of serpentinite, we expect that the ability for a serpentinite or serpentinite-dominated subduction channel to entrain and exhume other lithologies may also be time-dependent. As subduction matures, the progressive ingrowth of serpentinite weakens the interface more, meaning that return flow in a serpentinized subduction channel might be a more viable mechanism of exhumation after subduction reaches maturity and when the slabtop temperatures are generally lower than earlier stages. However, we do not observe large-scale exhumation in our models; additional mechanisms such as extensive surface erosion, greater channel buoyancy, or plate velocity changes (cf. England & Richardson, 1977; England & Smye, 2023; Ring et al., 1999) are likely needed.

Serpentinite is expected to be common along the plate interface, and therefore we expect that interface weakening is also tied to water release from hydrated lithologies, such as sediments, instead of inherently weak lithologies alone. A specific comparison to plate speeds is challenging because of other factors that affect subduction that include plate age, plate and trench geometry, overriding plate deformation, and forces associated with mantle flow (e.g., Isacks et al., 1968; Jagoutz et al., 2015; Lallemand et al., 2005; Ueda et al., 2008).

4.3. Model Limitations and Assumptions

Because we target the first-order impacts of serpentinization on subduction dynamics, and vice versa, some model simplification is necessary. The first set of assumptions pertains to initial conditions, model geometry, and numerical limitations. For example, model resolution modestly impacts the absolute quantities of serpentinite generated in the wedge. The current maximum model resolution is ~1.3 km; increasing the model resolution to 0.7 km increases instantaneous serpentinization by up to 15%, but the first-order trends remain unchanged (Figure S12 in Supporting Information S1). Additionally, we impose a MDD of 200 km by stiffening the crust (to the viscosity of the background mantle) at this depth. While this does not impact subduction zone thermal structure during the earlier subduction phases—during which the lower limit of the cold forearc much shallower—the incorporation of self-consistent, shallower decoupling depth would likely make the slabtop temperatures warmer (>30 Myr; Figure 4) and hence more compatible with mantle melting, arc volcanism, and surface heat flow during the mature phase (e.g., Furukawa, 1993; Wada & Wang, 2009). Finally, shear heating, not considered here, would also increase the slabtop temperature (e.g., England & Smye, 2023; Gao & Wang, 2014; Peacock, 1992; Penniston-Dorland et al., 2015) and may increase dehydration and serpentinization extents (Hernández-Uribe & Palin, 2019).

Care must also be taken in interpreting our models and others that make similar simplifying assumptions about the treatment of fluid flow and serpentinization. Free water is assumed to migrate directly upwards relative to the surrounding matrix, as is common in subduction modeling studies (e.g., Magni et al., 2014; Menant et al., 2019). However, channelization in the wedge or slab interface is possible, as suggested by stable isotope and trace element arguments from former interface units that have since been exhumed (e.g., Bebout & Penniston-Dorland, 2016; Epstein et al., 2021) and modeling studies with coupled deformation and porous fluid flow (Cerpa & Wada, 2025; Wilson et al., 2014). This assumption may impact the absolute quantities of serpentinite that our models predict. For example, after 50 Myr, our models predict the ingrowth of \sim 20% of instantaneous serpentinite of the Epstein et al. (2024) models, which assume perfect vertical transfer of fluids. Additionally, the hydration process we chose is designed to be conservative by requiring that 100% of a cell be serpentinized before any higher cells are affected, as suggested by the presence of H_2O being the primary limiting factor to serpentinization (Peacock, 1987). Upward-migrating swarms of earthquakes—likely indicating channelized fluid migration—suggest that not all fluid is immediately bound through reaction with peridotite upon reaching the wedge, and partial serpentinization is possible (Davies, 1999; Halpaap et al., 2019).

We rely on a closed-system equilibrium thermodynamic model to determine fluid release and flow laws during progressive subduction. Such models do not account for reaction overstepping, and are calculated in a closed system domain for all chemical components other than H_2O . Kinetic limitations to reactions shown by field studies (e.g., in exhumed wedge serpentinite: Peacock, 1987; in eclogite: Putnis & Austrheim, 2010) are not taken into account, and may influence the thermal-rheologic feedback. The assumption of a closed system for non-volatile components means that the initial composition has a significant control on dehydration systematics. For example, we assume the downgoing sediments are pelagic. Non-siliciclastic compositions, such as carbonate-rich sediments, undergo devolatilization to produce complex, mixed-volatile fluids, which may further weaken

STONER ET AL. 17 of 23

15252027, 2025, 11, Downloaded from https://agupubs.onlinelibrary.wiley.com/doi/10.1029/2025GC012488, Wiley Online Library on [16/11/2025]. See the Terms and Conditions (https://onlinelibrary.wiley.com/terms

Acknowledgments

This work was supported by NSF Grants

EAR-2119842 to Holt, EAR-2119843 to

thank Valeria Turino for helpful

discussions and for providing the

also thank the Computational Infrastructure for Geodynamics

Guevara, and EAR-2119844 to Condit. We

preprocessing script used in this study. We

organization (geodynamics.org), which is

funded by the National Science Foundation

under award EAR-0949446 and EAR-

of ASPECT. Computational resources

were provided by NSF ACCESS under

allocation EES-220058 to Holt.

1550901 for supporting the development

the plate interface (Oyanagi & Okamoto, 2024). Lastly, and, perhaps most importantly, we cannot model melt transport or fluid-induced metasomatic (i.e., open-system) reactions. Though weak hydrous minerals generated by metasomatism (Behnsen & Faulkner, 2012; Lindquist et al., 2023), such as talc and chlorite (Codillo et al., 2022; Easthouse et al., 2025; Klein & Behn, 2025; Oyanagi & Okamoto, 2024; Peacock & Wang, 2021; Shabtian & Hirth, 2025) are potentially less abundant than serpentine, they are considerably weaker than serpentine and may therefore exert a significant effect on plate strength. Overall, interface strength, plate speeds, and slab temperatures will evolve as weak, hydrous lithologies accumulate along the interface (Figure 9).

5. Conclusions

This study tracks serpentine buildup in the mantle wedge during subduction to reveal feedbacks between slab dehydration/forearc hydration, plate kinematics, dehydration, and slab thermal state over time. Feedbacks are included by allowing plate geometries and velocities to evolve freely within dynamic models, thereby capturing the highly time-dependent effects of serpentinization on large-scale subduction. Our models suggest:

- 1. As the downgoing plate dehydrates, the mantle wedge is progressively serpentinized over the lifetime of the subduction zone.
- 2. Serpentinite accumulation is modulated by the balance between wedge hydration and downdragging along the interface due to coupling with the downgoing plate.
- 3. Serpentinite ingrowth elevates subduction zone convergence rates because it weakens the plate interface. This is particularly pronounced during the intermediate-to-mature phases of subduction after sufficient serpentinite has accumulated and reduced the interface strength.
- 4. Exhumation of serpentinites may be favored after subduction infancy, that is, once a sufficient quantity of serpentinite has accumulated in the mantle wedge.

Our work links two previously proposed hypotheses in subduction zone evolution: weakening of the interface due to the subduction of sediments and weakening of the interface due to the ingrowth of hydrous minerals. The lubricating effect of serpentinite likely acts in concert with that of subducted sediments, especially during the intermediate-to-mature phases of subduction.

Conflict of Interest

The authors declare no conflicts of interest relevant to this study.

Data Availability Statement

The parameter files, visualization scripts, and code to run the numerical models in the study are available on Zenodo with the GPL-2 license via Stoner et al. (2025).

References

Abers, G. A., Van Keken, P. E., & Hacker, B. R. (2017). The cold and relatively dry nature of mantle forearcs in subduction zones. *Nature Geoscience*, 10(5), 333–337. https://doi.org/10.1038/ngeo2922

Agard, P., Plunder, A., Angiboust, S., Bonnet, G., & Ruh, J. (2018). The subduction plate interface: Rock record and mechanical coupling (from long to short timescales). *Lithos*, 320–321, 537–566. https://doi.org/10.1016/j.lithos.2018.09.029

Angiboust, S., Wolf, S., Burov, E., Agard, P., & Yamato, P. (2012). Effect of fluid circulation on subduction interface tectonic processes: Insights from thermo-mechanical numerical modelling. Earth and Planetary Science Letters, 357–358, 238–248. https://doi.org/10.1016/j.epsl.2012.09.012

Arcay, D., Doin, M.-P., Tric, E., Bousquet, R., & de Capitani, C. (2006). Overriding plate thinning in subduction zones: Localized convection induced by slab dehydration. *Geochemistry, Geophysics, Geosystems*, 7(2), Q02007. https://doi.org/10.1029/2005GC001061

Arcay, D., Tric, E., & Doin, M.-P. (2005). Numerical simulations of subduction zones: Effect of slab dehydration on the mantle wedge dynamics. Physics of the Earth and Planetary Interiors, 149(1–2), 133–153. https://doi.org/10.1016/j.pepi.2004.08.020

Audet, P., & Bürgmann, R. (2014). Possible control of subduction zone slow-earthquake periodicity by silica enrichment. *Nature*, 510(7505), 389–392. https://doi.org/10.1038/nature13391

Audet, P., McLellan, M., & Bloch, W. (2025). Structure and serpentinization of the northern Cascadia mantle wedge corner from receiver function modelling. Canadian Journal of Earth Sciences, 62(4), 909–922. https://doi.org/10.1139/cjes-2024-0121

Balázs, A., Faccenna, C., Gerya, T., Ueda, K., & Funiciello, F. (2022). The dynamics of forearc–back-arc basin subsidence: Numerical models and observations from mediterranean subduction zones. *Tectonics*, 41(5), e2021TC007078. https://doi.org/10.1029/2021tc007078

Bangerth, W., Dannberg, J., Fraters, M., Gassmöller, R., Glerum, A., Heister, T., et al. (2023). Geodynamics/aspect: ASPECT 2.5.0 (version v2.5.0). Zenodo. https://doi.org/10.5281/ZENODO.8200213

Bebout, G. E., & Penniston-Dorland, S. C. (2016). Fluid and mass transfer at subduction interfaces—The field metamorphic record. *Lithos*, 240–243, 228–258. https://doi.org/10.1016/j.lithos.2015.10.007

STONER ET AL. 18 of 23

- Becker, T. W. (2006). On the effect of temperature and strain-rate dependent viscosity on global mantle flow, net rotation, and plate-driving forces. *Geophysical Journal International*, 167(2), 943–957. https://doi.org/10.1111/j.1365-246x.2006.03172.x
- Behnsen, J., & Faulkner, D. R. (2012). The effect of mineralogy and effective normal stress on frictional strength of sheet silicates. *Journal of Structural Geology*, 42, 49–61. https://doi.org/10.1016/j.jsg.2012.06.015
- Behr, W. M., & Becker, T. W. (2018). Sediment control on subduction plate speeds. Earth and Planetary Science Letters, 502, 166–173. https://doi.org/10.1016/j.epsl.2018.08.057
- Behr, W. M., & Bürgmann, R. (2021). What's down there? The structures, materials and environment of deep-seated slow slip and tremor. Philosophical Transactions of the Royal Society A, 379(2193), 20200218. https://doi.org/10.1098/rsta.2020.0218
- Behr, W. M., Holt, A. F., Becker, T. W., & Faccenna, C. (2022). The effects of plate interface rheology on subduction kinematics and dynamics. Geophysical Journal International, 230(2), 796–812. https://doi.org/10.1093/gji/ggac075
- Behr, W. M., & Platt, J. P. (2013). Rheological evolution of a Mediterranean subduction complex. *Journal of Structural Geology*, 54, 136–155. https://doi.org/10.1016/j.isg.2013.07.012
- Billen, M. I., & Arredondo, K. M. (2018). Decoupling of plate-asthenosphere motion caused by non-linear viscosity during slab folding in the transition zone. *Physics of the Earth and Planetary Interiors*, 281, 17–30. https://doi.org/10.1016/j.pepi.2018.04.011
- Billen, M. I., & Hirth, G. (2005). Newtonian versus non-Newtonian upper mantle viscosity: Implications for subduction initiation. *Geophysical Research Letters*, 32(19), L19304. https://doi.org/10.1029/2005g1023457
- Boneh, Y., Pec, M., & Hirth, G. (2023). High-pressure mechanical properties of talc: Implications for fault strength and slip processes. *Journal of Geophysical Research: Solid Earth*, 128(3), e2022JB025815. https://doi.org/10.1029/2022jb025815
- Burdette, E., & Hirth, G. (2022). Creep rheology of antigorite: Experiments at subduction zone conditions. *Journal of Geophysical Research:* Solid Earth, 127(7), e2022JB024260. https://doi.org/10.1029/2022jb024260
- Carpenter, B. M., Marone, C., & Saffer, D. M. (2009). Frictional behavior of materials in the 3D SAFOD volume. *Geophysical Research Letters*,
- 36(5), L05302. https://doi.org/10.1029/2008GL036660
 Cerpa, N. G., & Wada, I. (2025). Hydration state and updip fluid migration in the slab mantle. *Journal of Geophysical Research: Solid Earth*,
- 130(6), e2024JB030609. https://doi.org/10.1029/2024jb030609
- Čížková, H., & Bina, C. R. (2013). Effects of mantle and subduction-interface rheologies on slab stagnation and trench rollback. *Earth and Planetary Science Letters*, 379, 95–103. https://doi.org/10.1016/j.epsl.2013.08.011
- Cloos, M. (1985). Thermal evolution of convergent plate margins: Thermal modeling and reevaluation of isotopic Ar-ages for blueschists in the Franciscan complex of California. *Tectonics*, 4(5), 421–433. https://doi.org/10.1029/tc004i005p00421
- Codillo, E. A., Klein, F., & Marschall, H. R. (2022). Preferential formation of chlorite over talc during Si-metasomatism of ultramafic rocks in subduction zones. Geophysical Research Letters, 49(19), e2022GL100218. https://doi.org/10.1029/2022g1100218
- Condit, C. B., & French, M. E. (2022). Geologic evidence of lithostatic pore fluid pressures at the base of the subduction seismogenic zone. Geophysical Research Letters, 49(12), e2022GL098862. https://doi.org/10.1029/2022g1098862
- Condit, C. B., Guevara, V. E., Delph, J. R., & French, M. E. (2020). Slab dehydration in warm subduction zones at depths of episodic slip and tremor. Earth and Planetary Science Letters, 552, 116601. https://doi.org/10.1016/j.epsl.2020.116601
- Connolly, J. A. D. (2005). Computation of phase equilibria by linear programming: A tool for geodynamic modeling and its application to subduction zone decarbonation. *Earth and Planetary Science Letters*, 236(1–2), 524–541. https://doi.org/10.1016/j.epsl.2005.04.033
- Conrad, C. P., & Hager, B. H. (1999). The thermal evolution of an Earth with strong subduction zones. Geophysical Research Letters, 26(19), 3041–3044. https://doi.org/10.1029/1999GL005397
- Davies, J. H. (1999). The role of hydraulic fractures and intermediate-depth earthquakes in generating subduction-zone magmatism. *Nature*, 398(6723), 142–145. https://doi.org/10.1038/18202
- Dengo, C. A., & Logan, J. M. (1981). Implications of the mechanical and frictional behavior of serpentinite to seismogenic faulting. *Journal of Geophysical Research*, 86(B11), 10771–10782. https://doi.org/10.1029/JB086iB11p10771
- Douglas, D., Codillo, E., Epstein, G. S., Seltzer, C., Strobl, L., & Mallick, E. (2023). Geodynamic constraints on the stability of forearc serpentinite in the cold nose of the mantle wedge. In *AGU fall meeting abstracts* (Vol. 2023).DI21C-0023
- Douglas, D., Ito, G., Boston, B., Dunn, R., Naliboff, J., Wessel, P., et al. (2025). Magma-assisted flexure of Hawaiian lithosphere inferred from three-dimensional models of lithospheric flexure constrained by active source seismic data. *Journal of Geophysical Research: Solid Earth*, 130(6), e2024JB030376. https://doi.org/10.1029/2024jb030376
- Dragovic, B., Angiboust, S., & Tappa, M. J. (2020). Petrochronological close-up on the thermal structure of a paleo-subduction zone (W. Alps). Earth and Planetary Science Letters, 547, 116446. https://doi.org/10.1016/j.epsl.2020.116446
- Easthouse, G., Hoover, W., Teng, F.-Z., Condit, C., Pike, C., Wang, Z.-Z., et al. (2025). Formation of talc in the subduction interface: Mg isotopes demonstrate mg loss over si gain. *Geology*, 53(5), 398–403. https://doi.org/10.1130/g52538.1
- England, P. C., & Richardson, S. W. (1977). The influence of erosion upon the mineral facies of rocks from different metamorphic environments. *Journal of the Geological Society*, 134(2), 201–213. https://doi.org/10.1144/gsjgs.134.2.0201
- England, P. C., & Smye, A. J. (2023). Metamorphism and deformation on subduction interfaces: 1. Physical framework. Geochemistry, Geophysics, Geosystems, 24(1), e2022GC010644. https://doi.org/10.1029/2022gc010644
- Epstein, G. S., Bebout, G. E., & Angiboust, S. (2021). Fluid and mass transfer along transient subduction interfaces in a deep paleo-accretionary wedge (western alps). Chemical Geology, 559, 119920. https://doi.org/10.1016/j.chemgeo.2020.119920
- Epstein, G. S., Condit, C. B., Stoner, R. K., Holt, A. F., & Guevara, V. E. (2024). Evolving subduction zone thermal structure drives extensive forearc mantle wedge hydration. AGU Advances, 5(4), e2023AV001121. https://doi.org/10.1029/2023av001121
- Escartín, J., Hirth, G., & Evans, B. (2001). Strength of slightly serpentinized peridotites: Implications for the tectonics of oceanic lithosphere. Geology, 29(11), 197. https://doi.org/10.1130/0091-7613(2001)029<1023:sosspi>2.0.co;2
- Faccenda, M., Gerya, T. V., Mancktelow, N. S., & Moresi, L. (2012). Fluid flow during slab unbending and dehydration: Implications for intermediate-depth seismicity, slab weakening and deep water recycling. *Geochemistry, Geophysics, Geosystems*, 13(1). https://doi.org/10. 1029/2011gc003860
- Faccenna, C., Becker, T. W., Lucente, F. P., Jolivet, L., & Rossetti, F. (2001). History of subduction and back-arc extension in the central Mediterranean. *Geophysical Journal International*, 145(3), 809–820. https://doi.org/10.1046/j.0956-540x.2001.01435.x
- Fildes, R. A., & Billen, M. I. (2025). Linking visco-elasto-plastic modeling of recent slab deformation to present-day deep earthquakes. *Journal of Geophysical Research: Solid Earth*, 130(3), e2024JB029678. https://doi.org/10.1029/2024jb029678
- Frost, H. J., & Ashby, M. F. (1982). Deformation mechanism maps: The plasticity and creep of metals and ceramics. Pergamon Press.
- Fryer, P., Wheat, C. G., & Mottl, M. J. (1999). Mariana blueschist mud volcanism: Implications for conditions within the subduction zone. Geology, 27(2), 103–106. https://doi.org/10.1130/0091-7613(1999)027<0103:MBMVIF>2.3.CO;2

STONER ET AL. 19 of 23

//agupubs.onlinelibrary.wiley.com/doi/10.1029/2025GC012488, Wiley Online Library on [16/11/2025]. See the Terms

- Furukawa, Y. (1993). Depth of the decoupling plate interface and thermal structure under arcs. *Journal of Geophysical Research*, 98(B11), 20005–20013. https://doi.org/10.1029/93jb02020
- Gao, X., & Wang, K. (2014). Strength of stick-slip and creeping subduction megathrusts from heat flow observations. Science, 345(6200), 1038–1041. https://doi.org/10.1126/science.1255487
- Gassmöller, R., Lokavarapu, H., Heien, E., Puckett, E. G., & Bangerth, W. (2018). Flexible and scalable particle-in-cell methods with adaptive mesh refinement for geodynamic computations. *Geochemistry, Geophysics, Geosystems*, 19(9), 3596–3604. https://doi.org/10.1029/ 2018GC007508
- Gavrilenko, M., Krawczynski, M., Ruprecht, P., Li, W., & Catalano, J. G. (2019). The quench control of water estimates in convergent margin magmas. American Mineralogist. 104(7), 936–948. https://doi.org/10.2138/am-2019-6735
- Gerya, T., & Stöckhert, B. (2006). Two-dimensional numerical modeling of tectonic and metamorphic histories at active continental margins. International Journal of Earth Sciences, 95(2), 250–274. https://doi.org/10.1007/s00531-005-0035-9
- Gerya, T. V., Connolly, J. A. D., & Yuen, D. A. (2008). Why is terrestrial subduction one-sided? *Geology*, 36(1), 43–46. https://doi.org/10.1130/G24060A.1
- Gerya, T. V., & Meilick, F. I. (2011). Geodynamic regimes of subduction under an active margin: Effects of rheological weakening by fluids and melts. *Journal of Metamorphic Geology*, 29(1), 7–31. https://doi.org/10.1111/j.1525-1314.2010.00904.x
- Gerya, T. V., Stöckhert, B., & Perchuk, A. L. (2002). Exhumation of high-pressure metamorphic rocks in a subduction channel: A numerical simulation. *Tectonics*, 21(6), 1056. https://doi.org/10.1029/2002tc001406
- Glerum, A., Thieulot, C., Fraters, M., Blom, C., & Spakman, W. (2018). Nonlinear viscoplasticity in ASPECT: Benchmarking and applications to subduction. Solid Earth. 9(2), 267–294. https://doi.org/10.5194/se-9-267-2018
- Gorczyk, W., Willner, A. P., Gerya, T. V., Connolly, J. A. D., & Burg, J.-P. (2007). Physical controls of magmatic productivity at Pacific-type convergent margins: Numerical modelling. *Physics of the Earth and Planetary Interiors*, 163(1), 209–232. https://doi.org/10.1016/j.pepi.2007.
- Grima, A. G., & Becker, T. W. (2024). The role of continental heterogeneity on the evolution of continental plate margin topography at subduction zones. Earth and Planetary Science Letters, 642, 118856. https://doi.org/10.1016/j.epsl.2024.118856
- Hacker, B. R. (2008). H₂O subduction beyond arcs. Geochemistry, Geophysics, Geosystems, 9, Q03001. https://doi.org/10.1029/2007GC001707
 Hacker, B. R., & Christie, J. M. (1990). Brittle/ductile and plastic/cataclastic transitions in experimentally deformed and metamorphosed amphibolite. In A. G. Duba, W. B. Durham, J. W. Handin, & H. F. Wang (Eds.), The brittle-ductile transition in rocks, Geophysical Monograph Series (Vol. 56, pp. 127–147). American Geophysical Union. https://doi.org/10.1029/gm056p0127
- Halpaap, F., Rondenay, S., Perrin, A., Goes, S., Ottemöller, L., Austrheim, H., et al. (2019). Earthquakes track subduction fluids from slab source to mantle wedge sink. *Science Advances*, 5(4), eaav7369. https://doi.org/10.1126/sciadv.aav7369
- Hamilton, D. L., Burnham, C. W., & Osborn, E. F. (1964). The solubility of water and effects of oxygen fugacity and water content on crystallization in mafic magmas. *Journal of Petrology*, 5(1), 21–39. https://doi.org/10.1093/petrology/5.1.21
- Heister, T., Dannberg, J., Gassmöller, R., & Bangerth, W. (2017). High accuracy mantle convection simulation through modern numerical methods II: Realistic models and problems. *Geophysical Journal International*, 210(2), 833–851. https://doi.org/10.1093/gji/ggx195
- Hernández-Uribe, D., & Palin, R. M. (2019). A revised petrological model for subducted oceanic crust: Insights from phase equilibrium modelling. *Journal of Metamorphic Geology*, 37(6), 745–768. https://doi.org/10.1111/jmg.12483
- Hilairet, N., & Reynard, B. (2009). Stability and dynamics of serpentinite layer in subduction zone. *Tectonophysics*, 465(1–4), 24–29. https://doi.org/10.1016/j.tecto.2008.10.005
- Hirth, G., & Kohlstedt, D. (2003). Rheology of the upper mantle and the mantle wedge: A view from the experimentalists. In J. Eiler (Ed.), *Inside the subduction factory*, *Geophysical Monograph Series* (Vol. 138, pp. 83–105). American Geophysical Union. https://doi.org/10.1029/138em06
- Hirth, G., Teyssier, C., & Dunlap, J. W. (2001). An evaluation of quartzite flow laws based on comparisons between experimentally and naturally deformed rocks. *International Journal of Earth Sciences*, 90, 77–87. https://doi.org/10.1007/s005310000152
- Holland, T. J. B., & Powell, R. (2011). An improved and extended internally consistent thermodynamic dataset for phases of petrological interest, involving a new equation of state for solids. *Journal of Metamorphic Geology*, 29(3), 333–383. https://doi.org/10.1111/j.1525-1314.2010.
- Holt, A. F., & Condit, C. B. (2021). Slab temperature evolution over the lifetime of a subduction zone. *Geochemistry, Geophysics, Geosystems*, 22(6), e2020GC009476. https://doi.org/10.1029/2020gc009476
- Horn, H. M., & Deere, D. U. (1962). Frictional characteristics of minerals. *Géotechnique*, 12(4), 319–335. https://doi.org/10.1680/geot.1962.12. 4.319
- Hyndman, R. D., & Peacock, S. M. (2003). Serpentinization of the forearc mantle. Earth and Planetary Science Letters, 212(3-4), 417-432. https://doi.org/10.1016/s0012-821x(03)00263-2
- Isacks, B., & Molnar, P. (1971). Distribution of stresses in the descending lithosphere from a global survey of focal-mechanism solutions of mantle earthquakes. *Reviews of Geophysics*, 9(1), 103–174. https://doi.org/10.1029/rg009i001p00103
- Isacks, B., Oliver, J., & Sykes, L. R. (1968). Seismology and the new global tectonics. *Journal of Geophysical Research*, 73(18), 5855–5899. https://doi.org/10.1002/9781118782149.ch7
- Ito, E., Harris, D. M., & Anderson, A. T. (1983). Alteration of oceanic crust and geologic cycling of chlorine and water. Geochimica et Cosmochimica Acta, 47(9), 1613–1624. https://doi.org/10.1016/0016-7037(83)90188-6
- Iwamori, H. (2007). Transportation of H₂O beneath the Japan arcs and its implications for global water circulation. *Chemical Geology*, 239(3–4), 182–198. https://doi.org/10.1016/j.chemgeo.2006.08.011
- Jagoutz, O., Royden, L., Holt, A. F., & Becker, T. W. (2015). Anomalously fast convergence of India and Eurasia caused by double subduction. Nature Geoscience, 8(6), 475–478. https://doi.org/10.1038/ngeo2418
- Jarrard, R. D. (2003). Subduction fluxes of water, carbon dioxide, chlorine, and potassium. Geochemistry, Geophysics, Geosystems, 4(5), 8905. https://doi.org/10.1029/2002gc000392
- Julve, J., Barbot, S., Moreno, M., Tassara, A., Araya, R., Catalán, N., et al. (2024). Recurrence time and size of Chilean earthquakes influenced by geological structure. *Nature Geoscience*, 17(1), 79–87. https://doi.org/10.1038/s41561-023-01327-8
- Kameyama, M., Yuen, D. A., & Karato, S.-I. (1999). Thermal-mechanical effects of low-temperature plasticity (the Peierls mechanism) on the deformation of a viscoelastic shear zone. *Earth and Planetary Science Letters*, 168(1–2), 159–172. https://doi.org/10.1016/S0012-821X(99)
- Karato, S. I., & Wu, P. (1993). Rheology of the upper mantle: A synthesis. Science, 260, 771–778. https://doi.org/10.1126/science.260.5109.771
 Katz, R. F., Spiegelman, M., & Langmuir, C. H. (2003). A new parameterization of hydrous mantle melting. Geochemistry, Geophysics, Geosystems, 4(9), 1073. https://doi.org/10.1029/2002GC000433

STONER ET AL. 20 of 23

onlinelibrary.wiley.com/doi/10.1029/2025GC012488, Wiley Online Library on [16/11/2025].

- Kerswell, B. C., Kohn, M. J., & Gerya, T. V. (2021). Backarc lithospheric thickness and serpentine stability control slab-mantle coupling depths in subduction zones. Geochemistry, Geophysics, Geosystems, 22(6), e2020GC009304. https://doi.org/10.1029/2020gc009304
- Kimura, G., & Ludden, J. (1995). Peeling oceanic crust in subduction zones. *Geology*, 23(3), 217–220. https://doi.org/10.1130/0091-7613(1995) 023<0217:pocisz>2.3.co;2
- Kincaid, C., & Sacks, I. S. (1997). Thermal and dynamical evolution of the upper mantle in subduction zones. *Journal of Geophysical Research*, 102(B6), 12295–12315. https://doi.org/10.1029/96JB03553
- King, S. D., & Hager, B. H. (1990). The relationship between plate velocity and trench viscosity in Newtonian and power-law subduction calculations. Geophysical Research Letters, 17(13), 2409–2412. https://doi.org/10.1029/GL017i013p02409
- Kirby, S. H., Stein, S., Okal, E. A., & Rubie, D. C. (1996). Metastable mantle phase transformations and deep earthquakes in subducting oceanic lithosphere. *Reviews of Geophysics*, 34(2), 261–306. https://doi.org/10.1029/96rg01050
- Klein, B. Z., & Behn, M. D. (2025). The impact of mélange formation on the rheology and H₂O budget of the subduction zone interface, with implications for diapir nucleation. *Geophysical Research Letters*, 52(7), e2024GL113049. https://doi.org/10.1029/2024g1113049
- Kocks, U. F., Argon, A. S., & Ashby, M. F. (1975). Thermodynamics and kinetics of slip. Pergamon Press.
- Kronbichler, M., Heister, T., & Bangerth, W. (2012). High accuracy mantle convection simulation through modern numerical methods. Geophysical Journal International, 191(1), 12–29. https://doi.org/10.1111/j.1365-246X.2012.05609.x
- Lallemand, S., Heuret, A., & Boutelier, D. (2005). On the relationships between slab dip, back-arc stress, upper plate absolute motion, and crustal nature in subduction zones. *Geochemistry, Geophysics, Geosystems*, 6(9), Q09006. https://doi.org/10.1029/2005gc000917
- Lamb, S. (2006). Shear stresses on megathrusts: Implications for mountain building behind subduction zones. *Journal of Geophysical Research*, 111(B7), B07401, https://doi.org/10.1029/2005jb003916
- Lamb, S., & Davis, P. (2003). Cenozoic climate change as a possible cause for the rise of the Andes. Nature, 425, 792–797. https://doi.org/10.1038/nature02049
- Li, Z.-H., Gerya, T., & Connolly, J. A. D. (2019). Variability of subducting slab morphologies in the mantle transition zone: Insight from petrological-thermomechanical modeling. Earth-Science Reviews, 196, 102874. https://doi.org/10.1016/j.earscirev.2019.05.018
- Lindquist, P. C., Condit, C. B., Hoover, W. F., Hernández-Uribe, D., & Guevara, V. E. (2023). Metasomatism and slow slip: Talc production along the flat subduction plate interface beneath Mexico (Guerrero). Geochemistry, Geophysics, Geosystems, 24(8), e2023GC010981. https://doi.org/ 10.1029/2023GC010981
- Magni, V., Bouilhol, P., & van Hunen, J. (2014). Deep water recycling through time. *Geochemistry, Geophysics, Geosystems*, 15(11), 4203–4216. https://doi.org/10.1002/2014gc005525
- Menant, A., Angiboust, S., & Gerya, T. (2019). Stress-driven fluid flow controls long-term megathrust strength and deep accretionary dynamics. Scientific Reports, 9(1), 9714. https://doi.org/10.1038/s41598-019-46191-y
- Mitchell, A. L., Gaetani, G. A., O'Leary, J. A., & Hauri, E. H. (2017). H₂O solubility in basalt at upper mantle conditions. Contributions to Mineralogy and Petrology, 172(10), 85. https://doi.org/10.1007/s00410-017-1401-x
- Molnar, P., & England, P. (1990). Temperatures, heat flux, and frictional stress near major thrust faults. *Journal of Geophysical Research*, 95(B4), 4833–4856. https://doi.org/10.1029/JB095iB04p04833
- Moore, D. E., & Lockner, D. A. (2004). Crystallographic controls on the frictional behavior of dry and water-saturated sheet structure minerals. *Journal of Geophysical Research*, 109(B3), B034. https://doi.org/10.1029/2003jb002582
- Moore, D. E., Lockner, D. A., Ma, S., Summers, R., & Byerlee, J. D. (1997). Strengths of serpentinite gouges at elevated temperatures. *Journal of Geophysical Research*, 102(B7), 14787–14801. https://doi.org/10.1029/97JB00995
- Moreno, M., Haberland, C., Oncken, O., Rietbrock, A., Angiboust, S., & Heidbach, O. (2014). Locking of the Chile subduction zone controlled by fluid pressure before the 2010 earthquake. *Nature Geoscience*, 7(4), 292–296. https://doi.org/10.1038/ngeo2102
- Nakao, A., Iwamori, H., & Nakakuki, T. (2016). Effects of water transportation on subduction dynamics: Roles of viscosity and density reduction. Earth and Planetary Science Letters, 454, 178–191. https://doi.org/10.1016/j.epsl.2016.08.016
- Nakao, A., Iwamori, H., Nakakuki, T., Suzuki, Y. J., & Nakamura, H. (2018). Roles of hydrous lithospheric mantle in deep water transportation and subduction dynamics. Geophysical Research Letters, 45(11), 5336–5343. https://doi.org/10.1029/2017GL076953
- Nikolaeva, K., Gerya, T. V., & Connolly, J. A. D. (2008). Numerical modelling of crustal growth in intraoceanic volcanic arcs. *Physics of the Earth and Planetary Interiors*, 171(1–4), 336–356. https://doi.org/10.1016/j.pepi.2008.06.026
- Oyanagi, R., & Okamoto, A. (2024). Subducted carbon weakens the forearc mantle wedge in a warm subduction zone. *Nature Communications*, 15(1), 7159. https://doi.org/10.1038/s41467-024-51476-6
- Peacock, S. M. (1987). Creation and preservation of subduction-related inverted metamorphic gradients. *Journal of Geophysical Research*, 92(B12), 12763–12781. https://doi.org/10.1029/jb092ib12p12763
- Peacock, S. M. (1990). Numerical simulation of metamorphic pressure-temperature-time paths and fluid production in subducting slabs. *Tectonics*, 9(5), 1197–1211. https://doi.org/10.1029/tc009i005p01197
- Peacock, S. M. (1992). Blueschist-facies metamorphism, shear heating, and P-T-t paths in subduction shear zones. *Journal of Geophysical Research*, 97(B12), 17693–17707. https://doi.org/10.1029/92JB01768
- Peacock, S. M., Christensen, N. I., Bostock, M. G., & Audet, P. (2011). High pore pressures and porosity at 35 km depth in the Cascadia subduction zone. *Geology*, 39(5), 471–474. https://doi.org/10.1130/g31649.1
- Peacock, S. M., & Wang, K. (2021). On the stability of talc in subduction zones: A possible control on the maximum depth of decoupling between the subducting plate and mantle wedge. *Geophysical Research Letters*, 48(17), e2021GL094889. https://doi.org/10.1029/2021gl094889
- Penniston-Dorland, S. C., Kohn, M. J., & Manning, C. E. (2015). The global range of subduction zone thermal structures from exhumed blueschists and eclogites: Rocks are hotter than models. *Earth and Planetary Science Letters*, 428, 243–254. https://doi.org/10.1016/j.epsl. 2015.07.031
- Penniston-Dorland, S. C., Wada, I., Raia, N. H., Steele, A., Bullock, E. S., Zhou, X., et al. (2025). Constraining the thermal structure of the subduction plate interface: Coupled petrologic and geodynamic study of high-pressure rocks of New Caledonia. Earth and Planetary Science Letters, 652, 119172. https://doi.org/10.1016/j.epsl.2024.119172
- Pitzer, K. S., & Sterner, S. M. (1994). Equations of state valid continuously from zero to extreme pressures for H₂O and CO₂. The Journal of Chemical Physics, 101(4), 3111–3116. https://doi.org/10.1063/1.467624
- Plank, T., & Langmuir, C. H. (1998). The chemical composition of subducting sediment and its consequences for the crust and mantle. *Chemical Geology*, 145(3–4), 325–394. https://doi.org/10.1016/S0009-2541(97)00150-2
- Platt, J. P. (1975). Metamorphic and deformational processes in the Franciscan Complex, California: Some insights from the Catalina Schist terrane. Geological Society of America Bulletin, 86(10), 1337–1347. https://doi.org/10.1130/0016-7606(1975)86<1337:madpit>2.0.co;2
- Podolefsky, N. S., Zhong, S., & McNamara, A. K. (2004). The anisotropic and rheological structure of the oceanic upper mantle from a simple model of plate shear. Geophysical Journal International, 158(1), 287–296. https://doi.org/10.1111/j.1365-246x.2004.02250.x

STONER ET AL. 21 of 23

15252027, 2025, 11, Downloaded

onlinelibrary.wiley.com/doi/10.1029/2025GC012488, Wiley Online Library on [16/11/2025]. See the Terms.

- Pusok, A. E., Stegman, D. R., & Kerr, M. (2022). The effect of low-viscosity sediments on the dynamics and accretionary style of subduction margins. Solid Earth, 13(9), 1455–1473. https://doi.org/10.5194/se-13-1455-2022
- Putnis, A., & Austrheim, H. (2010). Fluid-induced processes: Metasomatism and metamorphism. *Geofluids*, 10(1–2), 254–269. https://doi.org/10.1111/j.1468-8123.2010.00285.x
- Raleigh, C. B., & Paterson, M. S. (1965). Experimental deformation of serpentinite and its tectonic implications. *Journal of Geophysical Research*, 70(16), 3965–3985. https://doi.org/10.1029/jz070i016p03965
- Ranero, C. R., Phipps Morgan, J., McIntosh, K., & Reichert, C. (2003). Bending-related faulting and mantle serpentinization at the Middle America trench. *Nature*, 425, 367–373. https://doi.org/10.1038/nature01961
- Reinen, L. A., Weeks, J. D., & Tullis, T. E. (1994). The frictional behavior of lizardite and antigorite serpentinites: Experiments, constitutive models, and implications for natural faults. *Pure and Applied Geophysics*, 143(1–3), 317–358. https://doi.org/10.1007/bf00874334
- Ring, U., Brandon, M. T., Willett, S. D., & Lister, G. S. (1999). Exhumation processes. In U. Ring, M. T. Brandon, S. D. Willett, & G. S. Lister (Eds.), Exhumation processes: Normal faulting, ductile flow, and erosion (Vol. 154, pp. 1–27). Geological Society, London, Special Publications. https://doi.org/10.1144/GSL.SP.1999.154.01.01
- Ritter, S., Balázs, A., Ribeiro, J., & Gerya, T. (2024). Magmatic fingerprints of subduction initiation and mature subduction: Numerical modelling and observations from the izu-bonin-mariana system. Frontiers in Earth Science, 12, 1286468. https://doi.org/10.3389/feart.2024.1286468
- Rose, I., Buffett, B., & Heister, T. (2017). Stability and accuracy of free surface time integration in viscous flows. *Physics of the Earth and Planetary Interiors*, 262, 90–100. https://doi.org/10.1016/j.pepi.2016.11.007
- Rowe, C. D., Moore, J. C., Remitti, F., & IODP Expedition 343/343T Scientists. (2013). The thickness of subduction plate boundary faults from the seafloor into the seismogenic zone. *Geology*, 41(9), 991–994. https://doi.org/10.1130/g34556.1
- Rüpke, L. H., Morgan, J. P., Hort, M., & Connolly, J. A. D. (2004). Serpentine and the subduction zone water cycle. Earth and Planetary Science Letters, 223(1–2), 17–34. https://doi.org/10.1016/j.epsl.2004.04.018
- Rutter, E. H. (1976). A discussion on natural strain and geological structure-the kinetics of rock deformation by pressure solution. *Philosophical Transactions of the Royal Society of London Series A: Mathematical and Physical Sciences*, 283(1312), 203–219.
- Savov, I. P., Ryan, J. G., D'Antonio, M., & Fryer, P. (2007). Shallow slab fluid release across and along the Mariana arc-basin system: Insights from geochemistry of serpentinized peridotites from the Mariana fore arc. *Journal of Geophysical Research*, 112(B9), B09205. https://doi.org/10.1029/2006ib004749
- Scambelluri, M., Cannaò, E., & Gilio, M. (2019). The water and fluid-mobile element cycles during serpentinite subduction. A review. European Journal of Mineralogy, 31(3), 405–428. https://doi.org/10.1127/ejm/2019/0031-2842
- Scambelluri, M., & Tonarini, S. (2012). Boron isotope evidence for shallow fluid transfer across subduction zones by serpentinized mantle. Geology, 40(10), 907–910. https://doi.org/10.1130/G33233.1
- Schmidt, M. W., & Poli, S. (1998). Experimentally based water budgets for dehydrating slabs and consequences for arc magma generation. Earth and Planetary Science Letters, 163(1-4), 361-379. https://doi.org/10.1016/S0012-821X(98)00142-3
- Schwartz, S., Allemand, P., & Guillot, S. (2001). Numerical model of the effect of serpentinites on the exhumation of eclogitic rocks: Insights from the Monviso ophiolitic massif (Western Alps). *Tectonophysics*, 342(1–2), 193–206. https://doi.org/10.1016/s0040-1951(01)00162-7
- Scuderi, M. M., & Carpenter, B. M. (2022). Frictional stability and hydromechanical coupling of serpentinite-bearing fault gouge. Geophysical Journal International, 231(1), 290–305. https://doi.org/10.1093/gji/ggac188
- Sdrolias, M., & Müller, R. D. (2006). Controls on back-arc basin formation. Geochemistry, Geophysics, Geosystems, 7(4), Q04016. https://doi.org/10.1029/2005gc001090
- Shabtian, H. S., & Hirth, G. (2025). Creep of talc at subduction zone conditions: Implications for slow slip and strength of the lithosphere. Geophysical Research Letters, 52(19), e2025GL116641. https://doi.org/10.1029/2025g1116641
- Shreve, R. L., & Cloos, M. (1986). Dynamics of sediment subduction, melange formation, and prism accretion. *Journal of Geophysical Research*, 91(B10), 10229–10245. https://doi.org/10.1029/jb091ib10p10229
- Stein, C. A., & Stein, S. (1992). A model for the global variation in oceanic depth and heat flow with lithospheric age. *Nature*, 359, 123–129. https://doi.org/10.1038/359123a0
- Stoner, R. K., Holt, A. F., Epstein, G. S., Condit, C. B., & Guevara, V. E. (2025). ryanstoner1/aspect: V0.1.3-alpha (v0.1.3-alpha). Zenodo. https://doi.org/10.5281/zenodo.15345801
- Tatsumi, Y. (1986). Formation of the volcanic front in subduction zones. *Geophysical Research Letters*, 13(8), 717–720. https://doi.org/10.1029/g1013i008p00717
- Tatsumi, Y., & Eggins, S. (1995). Subduction zone magmatism. In *Subduction zone magmatism*. Blackwell Science; Frontiers in Earth Sciences. Tesei, T., Harbord, C. W. A., De Paola, N., Collettini, C., & Viti, C. (2018). Friction of mineralogically controlled serpentinites and implications for fault weakness. *Journal of Geophysical Research: Solid Earth*, 123(8), 6976–6991. https://doi.org/10.1029/2018JB016058
- Tonarini, S., Leeman, W. P., & Leat, P. T. (2011). Subduction erosion of forearc mantle wedge implicated in the genesis of the South sandwich island (SSI) arc: Evidence from boron isotope systematics. *Earth and Planetary Science Letters*, 301(1–2), 275–284. https://doi.org/10.1016/j.epsl.2010.11.008
- Tulley, C. J., ten Thij, L., Niemeijer, A. R., Hamers, M. F., & Fagereng, Å. (2024). Activation of dissolution-precipitation creep causes weakening and viscous behavior in experimentally deformed antigorite. *Journal of Geophysical Research: Solid Earth*, 129(8), e2024JB029053. https://doi.org/10.1029/2024jb029053
- Turino, V., & Holt, A. F. (2024). Spatio-temporal variability in slab temperature within dynamic 3-D subduction models. Geophysical Journal International, 236(3), 1484–1498. https://doi.org/10.1093/gji/ggad489
- Ueda, K., Gerya, T., & Sobolev, S. V. (2008). Subduction initiation by thermal–chemical plumes: Numerical studies. *Physics of the Earth and Planetary Interiors*, 171(1–4), 296–312. https://doi.org/10.1016/j.pepi.2008.06.032
- van Keken, P. E., Hacker, B. R., Syracuse, E. M., & Abers, G. A. (2011). Subduction factory: 4. Depth-dependent flux of H₂O from subducting slabs worldwide. *Journal of Geophysical Research*, 116(B1), B01401. https://doi.org/10.1029/2010jb007922
- Wada, I., Behn, M. D., & Shaw, A. M. (2012). Effects of heterogeneous hydration in the incoming plate, slab rehydration, and mantle wedge hydration on slab-derived H₂O flux in subduction zones. *Earth and Planetary Science Letters*, 353–354, 60–71. https://doi.org/10.1016/j.epsl. 2012.07.025
- Wada, I., & Wang, K. (2009). Common depth of slab-mantle decoupling: Reconciling diversity and uniformity of subduction zones. Geochemistry, Geophysics, Geosystems, 10(10), Q10009. https://doi.org/10.1029/2009gc002570
- Wada, I., Wang, K., He, J., & Hyndman, R. D. (2008). Weakening of the subduction interface and its effects on surface heat flow, slab dehydration, and mantle wedge serpentinization. *Journal of Geophysical Research*, 113(B4), B04402. https://doi.org/10.1029/2007jb005190
- Wang, K., Hyndman, R. D., & Yamano, M. (1995). Thermal regime of the Southwest Japan subduction zone: Effects of age history of the subducting plate. Tectonophysics, 248(1-2), 53-69. https://doi.org/10.1016/0040-1951(95)00028-1

STONER ET AL. 22 of 23

onlinelibrary.wiley.com/doi/10.1029/2025GC012488, Wiley Online Library on [16/11/2025].

conditions) on Wiley Online Library for rules of use; OA articles are governed by the applicable Creative Cor

- Wilson, C. R., Spiegelman, M., van Keken, P. E., & Hacker, B. R. (2014). Fluid flow in subduction zones: The role of solid rheology and compaction pressure. Earth and Planetary Science Letters, 401, 261–274. https://doi.org/10.1016/j.epsl.2014.05.052
- Zhang, J., & Green, H. W. (2007). Experimental investigation of eclogite rheology and its fabrics at high temperature and pressure. *Journal of Metamorphic Geology*, 25(2), 97–115. https://doi.org/10.1111/j.1525-1314.2006.00684.x
- Zhou, X., & Wada, I. (2021). Differentiating induced versus spontaneous subduction initiation using thermomechanical models and metamorphic soles. Nature Communications, 12(1), 4632. https://doi.org/10.1038/s41467-021-24896-x

References From the Supporting Information

- Amiguet, E., Van De Moortèle, B., Cordier, P., Hilairet, N., & Reynard, B. (2014). Deformation mechanisms and rheology of serpentines in experiments and in nature. *Journal of Geophysical Research: Solid Earth*, 119(6), 4640–4655. https://doi.org/10.1002/2013JB010791
- Auzanneau, E., Schmidt, M. W., Vielzeuf, D., & Connolly, J. A. D. (2010). Titanium in phengite: A geobarometer for high temperature eclogites. Contributions to Mineralogy and Petrology, 159(1), 1–24. https://doi.org/10.1007/s00410-009-0412-7
- Chernak, L. J., & Hirth, G. (2010). Deformation of antigorite serpentinite at high temperature and pressure. Earth and Planetary Science Letters, 296(1–2), 23–33. https://doi.org/10.1016/j.epsl.2010.04.035
- Coggon, R., & Holland, T. J. B. (2002). Mixing properties of phengitic micas and revised garnet-phengite thermobarometers. *Journal of Metamorphic Geology*, 20(7), 683–696. https://doi.org/10.1046/j.1525-1314.2002.00395.x
- Connolly, J. A. D., & Trommsdorff, V. (1991). Petrogenetic grids for metacarbonate rocks: Pressure-temperature phase-diagram projection for mixed-volatile systems. Contributions to Mineralogy and Petrology, 108(1–2), 93–105. https://doi.org/10.1007/BF00307329
- Escartín, J., Hirth, G., & Evans, B. (1997). Effects of serpentinization on the lithospheric strength and the style of normal faulting at slow-spreading ridges. Earth and Planetary Science Letters, 151(3-4), 181-189. https://doi.org/10.1016/s0012-821x(97)81847-x
- Fuhrman, M. L., & Lindsley, D. H. (1988). Ternary-feldspar modeling and thermometry. American Mineralogist, 73(3-4), 201-215. https://doi.org/10.1007/s00410-009-0480-8
- Green, E. C. R., Holland, T. J. B., & Powell, R. (2007). An order-disorder model for omphacitic pyroxenes in the system jadeite-diopside-hedenbergite-acmite, with applications to eclogitic rocks. *American Mineralogist*, 92(7), 1181–1189. https://doi.org/10.2138/am.2007.2401
- Green, E. C. R., White, R. W., Diener, J. F. A., Powell, R., Holland, T. J. B., & Palin, R. M. (2016). Activity-composition relations for the calculation of partial melting equilibria in metabasic rocks. *Journal of Metamorphic Geology*, 34(9), 845–869. https://doi.org/10.1111/jmg.
- Hilairet, N., Reynard, B., Wang, Y., Daniel, I., Merkel, S., Nishiyama, N., & Petitgirard, S. (2007). High-pressure creep of serpentine, interseismic deformation, and initiation of subduction. Science, 318, 1910–1913. https://doi.org/10.1126/science.1148494
- Holland, T. J. B., Green, E. C. R., & Powell, R. (2018). Melting of peridotites through to granites: A simple thermodynamic model in the system KNCFMASHTOCr. Journal of Petrology, 59(5), 881–900. https://doi.org/10.1093/petrology/egy048
- Holland, T. J. B., Hudson, N. F., Powell, R., & Harte, B. (2013). New thermodynamic models and calculated phase equilibria in NCFMAS for basic and ultrabasic compositions through the transition zone into the uppermost lower mantle. *Journal of Petrology*, 54(9), 1901–1920. https://doi.org/10.1093/petrology/egt035
- Jennings, E. S., & Holland, T. J. B. (2015). A simple thermodynamic model for melting of peridotite in the system NCFMASOCr. *Journal of Petrology*, 56(5), 869–892. https://doi.org/10.1093/petrology/egv020
- Kawano, S., Katayama, I., & Okazaki, K. (2011). Permeability anisotropy of serpentinite and fluid pathways in a subduction zone. Geology, 39(10), 939–942. https://doi.org/10.1130/g32173.1
- Moore, D. E., Lockner, D. A., Summers, R., Shengli, M. A., & Byerlee, J. D. (1996). Strength of chrysotile-serpentinite gouge under hydrothermal conditions: Can it explain a weak San Andreas fault? *Geology*, 24(11), 1041–1044. https://doi.org/10.1130/0091-7613(1996)024<1041: socsgu>2.3.co;2
- Padrón-Navarta, J. A., Sánchez-Vizcaíno, V. L., Hermann, J., Connolly, J. A., Garrido, C. J., Gómez-Pugnaire, M. T., & Marchesi, C. (2013). Tschermak's substitution in antigorite and consequences for phase relations and water liberation in high-grade serpentinites. *Lithos*, 178, 186–196. https://doi.org/10.1016/j.lithos.2013.02.001
- Tajčmanová, L., Connolly, J. A. D., & Cesare, B. (2009). A thermodynamic model for titanium and ferric iron solution in biotite. *Journal of Metamorphic Geology*, 27(2), 153–165. https://doi.org/10.1111/j.1525-1314.2009.00812.x
- Tarling, M. S., Smith, S. A. F., Scott, J. M., Rooney, J. S., Viti, C., & Gordon, K. C. (2019). The internal structure and composition of a plate-boundary-scale serpentinite shear zone: The livingstone fault, New Zealand. Solid Earth, 10(4), 1025–1047. https://doi.org/10.5194/se-10-1025-2019
- White, R. W., Pomroy, N. E., & Powell, R. (2005). An in situ metatexite-diatexite transition in upper amphibolite facies rocks from Broken Hill, Australia. Journal of Metamorphic Geology, 23(7), 579–602. https://doi.org/10.1111/j.1525-1314.2005.00597.x
- White, R. W., Powell, R., Holland, T. J. B., Johnson, T. E., & Green, E. C. R. (2014). New mineral activity–composition relations for thermodynamic calculations in metapelitic systems. *Journal of Metamorphic Geology*, 32(3), 261–286. https://doi.org/10.1111/jmg.12071

STONER ET AL. 23 of 23